Anti-capsule human monoclonal antibodies protect against hypervirulent and pandrug-resistant *Klebsiella pneumoniae*

Emanuele Roscioli[1,12], Vittoria Zucconi Galli Fonseca[1,2,12], Soraya Soledad Bosch[1,12], Ida Paciello[1], Giuseppe Maccari[3], Giampiero Batani[1], Samuele Stazzoni[1], Giulia Cardinali[1,2], Giusy Tiseo[4], Cesira Giordano[5], Yuwei Shen[6], Laura Capoccia[1,7], Matteo Ridelfi[1,2], Marco Troisi[1], Noemi Manganaro[1], Chiara Mugnaini[1], Dario Cardamone[3], Concetta De Santi[1], Annalisa Ciabattini[7], Linda Cerofolini[8], Marco Fragai[8], Danilo Licastro[9], David P. Nicolau[6], Kamilia Abdelraouf[6], Simona Barnini[5], Francesco Menichetti[4], Marco Falcone[4], Claudia Sala[1,13], Anna Kabanova[1,10,13,*], Rino Rappuoli[11,13,*]

[1] Monoclonal Antibody Discovery (MAD) Lab, Fondazione Toscana Life Sciences, Siena, Italy
[2] Department of Biotechnology, Chemistry and Pharmacy, University of Siena, Siena, Italy
[3] Data Science for Health (DASCH) Lab, Fondazione Toscana Life Sciences, Siena, Italy
[4] Department of Clinical and Experimental Medicine, Infectious Diseases Unit, University of Pisa, Pisa, Italy
[5] Microbiology Unit, Azienda Universitaria Ospedaliera Pisana, Pisa, Italy
[6] Center for Anti-infective Research and Development, Hartford Hospital, Hartford, CT, US
[7] Department of Medical Biotechnologies, University of Siena, Siena, Italy
[8] Magnetic Resonance Center (CERM), University of Florence, and Consorzio Interuniversitario Risonanze Magnetiche di Metalloproteine (CIRMMP), Sesto Fiorentino, Italy
[9] AREA Science Park, Padriciano, Trieste, Italy
[10] Tumor Immunology Unit, Fondazione Toscana Life Sciences, Siena, Italy
[11] Fondazione Biotecnopolo di Siena, Siena, Italy
[12] These authors contributed equally
[13] Senior author
*Correspondence: rino.rappuoli@biotecnopolo.it; a.kabanova@toscanalifesciences.org

SUMMARY

The silent pandemic caused by antimicrobial resistance (AMR) requires innovative therapeutic approaches. Human monoclonal antibodies (mAbs), which are among the most transformative, safe and effective drugs in oncology and autoimmunity, are rarely used for infectious diseases and not yet used for AMR. Here we applied an antigen-agnostic strategy to isolate extremely potent human mAbs against *Klebsiella pneumoniae* (Kp) sequence type 147 (ST147), a hypervirulent and pandrug-resistant clonotype which is spreading globally. Isolated mAbs target the bacterial capsule and the O-antigen. Surprisingly, although both capsule- and O-antigen-specific mAbs displayed bactericidal activity in the picomolar range *in vitro*, only the capsule-specific mAbs were protective against fulminant ST147 bloodstream infection. Protection correlated with *in vitro* bacterial uptake by macrophages and enchained bacterial growth. Our study describes the only drug able to protect against pandrug-resistant Kp and provides a strategy to isolate mAbs and identify correlates of protection against AMR bacteria.

KEYWORDS

Klebsiella pneumoniae; Human monoclonal antibodies; pandrug-resistant bacteria; AMR; capsule locus 64; KL64; ST147.

53 INTRODUCTION

54

55 Antimicrobial resistance (AMR) has been enlisted by the World Health Organization, the
56 European Medicines Agency and the United Nations as one of the top ten global health priorities,
57 due to its impact on human health and socio-economic welfare worldwide[1]. Among AMR
58 pathogens, *Enterobacteriaceae* causing threats in hospital settings are considered the most
59 critical[2] and are currently dominated by *Klebsiella pneumoniae* (Kp) species[3]. Most Kp strains that
60 cause severe infections belong to two major pathotypes, namely the classical and hypervirulent
61 ones[4]. Classical Kp is a frequent cause of healthcare-associated infections and can easily acquire
62 mobile genetic elements associated with AMR[5]. In particular, multidrug-resistant Kp strains
63 carrying extended-spectrum β-lactamases and carbapenemases have played a major role in
64 global AMR spread. Among carbapenemases, the New Delhi Metallo-β-lactamases (NDM) are
65 extremely alarming since they confer resistance to the most recent combinations of β-lactams
66 and β-lactamase inhibitors (i.e., ceftazidime–avibactam, imipenem–relebactam, and
67 meropenem–vaborbactam), which are considered the last line of defense[6]. NDMs are encoded
68 by bla_{NDM} genes located on large multi-resistance plasmids that have been spreading across high-
69 risk AMR Kp clones throughout all continents[7,8]. On the other hand, hypervirulent Kp (hvKp)
70 isolates carry large virulence plasmids encoding genes related to capsule synthesis and
71 siderophore production[4]. Despite showing higher susceptibility to antimicrobial agents, hvKp
72 strains can cause severe community-acquired infections, such as pyogenic liver abscess,
73 endophthalmitis, and meningitis[7–10], even in healthy individuals.
74 Although hypervirulence and multidrug resistance have evolved distinctly within Kp, convergence
75 of both traits has been described recently, particularly in extensively drug resistant NDM-
76 producing Kp strains[11]. Notably, an NDM-1-positive sequence type 147 ($ST147_{NDM-1}$) Kp strain
77 carrying both AMR and hypervirulence genes has been disseminating globally[12–14] since mid-late
78 2000s and was associated with acquisition of carbapenemase-encoding genes in various
79 countries[12–14]. The only antibiotic to which $ST147_{NDM-1}$ is still sensitive is colistin which is
80 associated with high systemic toxicity and is used as the last resort treatment for AMR infection[15–
81 17]. Today, ST147 accounts for about 5% of Kp infections worldwide[18]. In 2018[19–21] ST147 isolate

82 landed in Tuscany (Italy), causing a nosocomial outbreak associated with a 30-day mortality rate
83 close to 40%[19]. Genomic surveillance data indicate that ST147 isolates from the Tuscany outbreak
84 carry a highly diversified plasmid content[19], bearing numerous AMR genes and virulence factors.
85 Similar genetic rearrangements had been already detected in Russia (2017)[22], United Kingdom
86 (2018-2019)[23] Egypt (2019)[24], and in the 2019 Kp outbreak in Germany[25], where different Kp STs
87 coharbouring virulence genes and bla_{NDM} were reported. Indeed, an ancestor of the Tuscany
88 outbreak strain[20] has been recently classified as pandrug-resistant (PDR)[26,27], leaving scarce
89 therapeutic solutions against this pathogen.
90 Taking into consideration a scenario where high-risk Kp clones can cause catastrophic epidemics,
91 it is mandatory to search for effective treatment strategies. In this context, human monoclonal
92 antibodies (mAbs) represent a powerful tool that can rapidly progress to innovative prophylactic
93 and therapeutic solutions. Notably, mAbs are unique in having intrinsically good safety profiles
94 and avoiding impact on the host microbiota given their high specificity[28]. However, their use
95 against the AMR threat has been underexplored. In fact, while 26 mAbs against bacterial
96 pathogens have entered clinical phases for efficacy evaluation, only a few have gained FDA
97 approval[28], and none of them is directed against Kp.
98 At the preclinical level, several human and murine mAbs targeting Kp, but not $ST147_{NDM-1}$ strains,
99 have been reported. A few of these mAbs are directed against the capsular polysaccharide or the
100 O-antigen and both types have shown protective efficacy against ST258 Kp in a murine
101 intratracheal infection model[29,30] or in models of acutely lethal pneumonia by ATCC8045 Kp[31],
102 bacteremia by ST258[32] and O3a and O3b types of Kp (O3:K11)[33]. However, while the anti-capsule
103 antibodies are clearly associated with protection in some studies[34], the role of O-antigen
104 antibodies is still controversial because other studies reported that the O-antigen may not be
105 accessible to antibodies in capsulated strains[35,36]. Although valuable, the above findings find little
106 applicability to $ST147_{NDM-1}$ for one major reason: the astonishing variability of antigenic
107 polysaccharidic structures across Kp strains. Indeed, more than 100 capsule serotypes (K antigen)
108 have been described so far[37], while 11 distinct O-antigen serogroups exist, with four O-antigens
109 (O1, O2, O3, and O5) associated with 80-90% of Kp clinical isolates[4]. Moreover, continuous
110 diversification of O-antigen structures, such as addition of pyruvate to O1b[38] and GlcNAc to

111 O2ac[39], generates new epitopes. This imposes the development of serotype-specific mAbs or
112 cross-validation of the pre-existing ones. On the other hand, mAbs targeting the type III fimbrial
113 component MrkA were protective in a mouse model of lethal pneumonia caused by ATCC29011
114 Kp[40] and could find broader application as MrkA is conserved across various Kp strains. However,
115 another gap withholds their applicability against AMR Kp, specifically against the hypervirulent
116 and pandrug-resistant $ST147_{NDM-1}$: the lack of knowledge on the correlates of protection against
117 bloodstream infection. Most mAb development efforts have focused on target-specific
118 approaches, whereas no comprehensive studies comparing mAbs against larger panel of Kp
119 epitopes have been undertaken.
120 In this work, we describe a powerful method for unbiased mAb selection against $ST147_{NDM-1}$ not
121 bound to a particular predetermined antigen, which allowed the isolation of potent bactericidal
122 mAbs from donors that experienced $ST147_{NDM-1}$ bloodstream infection. By using a combination
123 of three high-throughput functional *in vitro* assays we defined functional properties of mAbs
124 associated with protection against fulminant bloodstream infection. Our study describes the first
125 fully human mAb against the hypervirulent and pandrug-resistant $ST147_{NDM-1}$ Kp lineage and
126 shows in a definitive manner that highly bactericidal anti O-antigen antibodies are not protective
127 against this hypervirulent and pandrug-resistant strain. This is an example of how a rationally
128 designed experimental pipeline allows to predict correlates of *in vivo* efficacy that could be
129 universally applied to other emerging AMR strains.
130
131
132

133 RESULTS

134

135 Isolation of bactericidal human mAbs against Tuscany outbreak strain $ST147_{NDM-1}$

136 To isolate Kp-specific mAbs representing the breadth of antibody repertoire induced by Kp
137 infection, an antigen-agnostic approach was used. Peripheral blood mononuclear cells (PBMCs)
138 were collected from 7 convalescent patients who recovered from $ST147_{NDM-1}$ Kp bloodstream
139 infection of the Tuscany nosocomial outbreak (**Table S1**). A total of 18,390 $CD19^{+}CD27^{+}IgM^{-}IgD^{-}$
140 memory B cells (MBCs), either IgG- or IgA-positive, was single-cell sorted and plated together
141 with CD40L-expressing feeder cells, IL-2 and IL-21 to promote MBCs activation, proliferation and
142 antibody secretion (**Figure 1A; Figure S1A**). MBCs culture supernatants were screened by
143 enzyme-linked immunosorbent assay (ELISA) against $ST147_{NDM-1}$ bacteria to select Kp-reactive
144 mAbs. 214 mAbs specific for antigens displayed on the bacterial surface were identified (**Figure**
145 **1B)**.

146 Upon molecular cloning of their V_H and V_L variable portions (**Table S2**), sequences of 134 Kp-
147 reactive mAbs were recovered with successful V_H and V_L pairing. To validate binding properties
148 of the isolated mAbs, they were expressed on a small scale and tested by ELISA against two
149 outbreak-belonging $ST147_{NDM-1}$ Kp isolates (**Figure S1B**). Further, mAbs were screened for their
150 ability to induce complement-dependent killing of $ST147_{NDM-1}$ Kp[41]. For this purpose, we
151 developed a high-throughput luminescence-based serum bactericidal assay (L-SBA) that
152 measures ATP content as a proxy of Kp viability[42,43]. Four dilutions per mAb were tested in the
153 presence of an exogenous source of complement and antibodies causing a reduction greater than
154 30% in bacterial viability were considered as positive hits. Out of the 134 Kp-binding mAbs
155 screened, 25 candidates showing bactericidal activity against $ST147_{NDM-1}$ were selected (**Figure**
156 **1C**) and expressed on the larger scale. Upon excluding five mAbs that failed to re-confirm their
157 bactericidal activity, binding and functional properties of the remaining 20 bactericidal $ST147_{NDM-}$
158 $_{1}$-targeting mAbs were evaluated.

159

160 Kp strain library profiling reveals that bactericidal mAbs display different degrees of cross-
161 reactivity and antigen specificity

162 To characterize specificity and cross-reactivity of the isolated bactericidal mAbs, flow cytometry
163 was employed to profile their binding against a panel of bacterial strains. Pathogenic Kp
164 belonging to different genetically distant STs were included (**Table 1, Figure S2A**), as well as other
165 *Klebsiella* species and several commensal strains. Antibody binding to bacterial surface displayed
166 different levels of intensity, suggesting differential expression of target antigens or variable
167 affinity of the mAbs (**Figure 2A**). Moreover, mAbs showed high specificity to pathogenic *sensu*
168 *stricto* Kp strains as they did not react with other *Klebsiella* species nor with commensals (**Figure**
169 **S2B**). Based on their binding profiles, mAbs were grouped into two main clusters. The first cluster
170 (c*luster 1*) encompassed mAbs with rather restricted binding features, recognizing exclusively the
171 outbreak strain ST147 carrying either $bla_{\text{NDM-1}}$ or $bla_{\text{NDM-9}}$ genes[44]. The second group of mAbs
172 (c*luster 2*) displayed a broader binding pattern, being able to recognize up to seven different
173 sequence types of pathogenic Kp (**Figure 2A**).

174 Comparative whole genome sequencing of the Kp strain library allowed inferring the surface
175 antigens targeted by the selected mAbs. Pangenome analysis of the isolates identified a subset
176 cluster of genes (COG) exclusively present in strains recognized by cluster 1 mAbs (**Table S3**).
177 Notably, COG associated with the KL64 locus of *wcaJ* was identified. WcaJ functions as the
178 initiating enzyme in the synthesis of colanic acid, a primary constituent of the capsule of
179 *Enterobacteriaceae*[45]. This finding aligned with the specificity of cluster 1 mAbs, which exclusively
180 recognized strains carrying genes belonging to the KL64 biosynthetic locus (**Figure 2A**)[46], thus
181 suggesting that their cognate antigen might be the capsule.

182 Regarding the putative target of cluster 2 mAbs, we observed that they reacted with Kp strains
183 belogning to different STs but displayed almost null binding to $ST147_{\text{NDM-9}}$ (**Figure 2A**). Therefore,
184 we assumed that these mAbs were very likely directed against a surface antigen lacking in the
185 $ST147_{\text{NDM-9}}$ isolate. Genomic analysis of the O-antigen biosynthetic loci revealed that $ST147_{\text{NDM-9}}$
186 presented a single-point deletion in position 474 of the *wbbO* gene (**Figure S3A**), which encodes
187 for a glycosyltransferase essential for O2a biosynthesis (**Figure S3B**)[47]. This mutation causes
188 frameshift and premature termination of translation likely hindering the production of the

189 complete O-antigen[48]. Indeed, HPLC and SDS-PAGE analyses of total sugar extracts from
190 $ST147_{NDM-9}$ confirmed that this strain was a natural O-antigen-deficient mutant when compared
191 to $ST147_{NDM-1}$ (**Figure S4A and B**). Thus, we hypothesized that cluster 2 mAbs recognized the
192 $ST147_{NDM-1}$ O-antigen. To confirm this, $ST147_{NDM-9}$ was transformed with a plasmid that carried
193 the wild type *wbbO* gene, or with the empty vector as a control. ELISA experiments demonstrated
194 that binding of cluster 2 mAbs was restored in the merodiploid strain $ST147_{NDM-9}$ *wbbO*$^{+}$, whilst
195 background-level signals were measured $ST147_{NDM-9}$ *wbbO*$^{-}$ carrying empty vector (**Figure 2B**).
196 Consistent with these results, immunoblotting analysis of total sugar extracts showed recognition
197 of $ST147_{NDM-9}$ *wbbO*$^{+}$ by the cluster 2 mAbs 05N02 (**Figure 2C)** and 05D08 (**Figure 2D**), while no
198 difference among strains was observed with the cluster 1 mAb 08O09 (**Figure 2E**). Overall, these
199 data confirmed successful complementation of $ST147_{NDM-9}$ and identification of the O-antigen as
200 the target of cluster 2 mAbs.
201
202 ## ST147-specific bactericidal mAbs target $ST147_{NDM-1}$ capsule and O-antigen
203 Biochemical validation of the mAb cognate antigens was sought by ELISA against purified Kp
204 capsule **(Figure S4C and D)** and O-antigens of various origins (**Figure S4E, F and G**). KL64 capsule
205 was recognized only by cluster 1 mAbs (**Figure 2F**). Moreover, immunoblotting of Kp total sugar
206 extract further confirmed that these antibodies decorated high molecular weight (MW)
207 structures of KL64-bearing Kp strains, in agreement with electrophoretic profiles of
208 polysaccharidic capsules[49] (**Figure 2G**).
209 Instead, ELISA against purified O-antigens revealed a more heterogeneous picture within cluster
210 2 mAbs. Three mAbs bound to purified LPS/O2a O-antigen, with variable degree of cross-
211 reactivity against O2afg and O1 O-antigens (**Figure 2F**). Their immunoblotting evidenced a ladder-
212 like binding pattern, compatible with typical O-antigen immunoblotting profiles[48] (**Figure 2H**).
213 Four other mAbs from cluster 2 did not recognize purified LPS or O-antigens in ELISA (**Figure 2F**).
214 However they displayed a similar ladder-like binding profile against total sugar extracts of Kp
215 strains expressing O2a O-antigens (**Figure 2I**)[48] and, as described in the previous paragraph,
216 successfully bound the *wbbO*-complemented $ST147_{NDM-9}$ strain (**Figure 2B and D**). Altogether,
217 these analyses allowed grouping bactericidal $ST147_{NDM-1}$-targeting antibodies into KL64-specific

218 and O2a O-antigen-specific mAbs, wherein some of the latter were found to be cross-reactive
219 against O2afg and O1 type O-antigen.
220 High-resolution and high-content imaging indicated that mAbs directed against capsule and O-
221 antigen displayed different localization patterns (**Figure 3A**). For instance, the anti-capsule mAb
222 08O09 showed higher intensity binding levels compared to the anti-O-antigen mAbs 05D08 and
223 05N02 (**Figure 3B)**. In addition, while 08O09 signal occupied a median area of 8.3±3.4 μm^2, 05D08
224 and 05N02 mAbs distributed over a smaller area of 4.9±1.6 μm^2 and 4.8±1.5 μm^2, respectively
225 (**Figure 3C**, **Figure S5**). Co-staining experiments with 08O09-A488 and 05N02-A555 conjugated
226 mAbs confirmed that 08O09 localized on the outermost layer of the bacteria (**Figure 3D**).
227 Whereas, in three-color assays, 05N02-A555 co-localized with 05D08-A647 and distributed more
228 internally than 08O09-A488 (**Figure 3E**), in agreement with differential specificity.
229

230 ## mAbs sequence analysis reflects functional clustering

231 Analysis of heavy (HC) and light chain (LC) mAb sequences revealed insights into their germline
232 composition. The genes encoding the HCs and LCs of 20 bactericidal mAbs were sequenced, and
233 their IGHV and IGKV genes were analyzed (**Figure S6A**). The most common HC V gene was *IGHV3-*
234 *23* (n=8, 40%), followed by *IGHV3-21* (n=3, 15%). The most prominent HC J gene was *IGHJ4* (n=15,
235 75%), mostly recombining with *IGHV3-23* (n=7, 35%), but showing diversity in the V gene. Most
236 of the selected mAbs used the κ chain (n=17, 85%), with only three out of 20 using the λ chain.
237 The light chain (LC) V gene usage was not as polarized as in the HC, with the *IGKV3-20* and the
238 *IGKV2-30* used by 30% of the mAbs (n=3+3). Similarly, the LC J gene did not show polarized usage,
239 with the most prominent V gene being *IGKJ1* (n=6; 30%), followed by *IGKJ2* (n=4, 20%). Initial
240 examination evidenced a bias in germline usage for anti-capsular mAbs, *with IGHV3-*
241 *23*04*;*IGHJ4*02* being the most common HC recombination (n=6, 30%) (**Figure S6B**), while two
242 clonal pairs were detected among O-antigen-specific mAbs (*IGHV3-15*01*;*IGHJ4*02*, *IGHV1-*
243 *18*01*;*IGHJ4*02*) (**Table S4**). To further investigate sequence relationships, the heavy and light
244 chain sequences were analyzed separately using Clustal Omega, and sequence distances were
245 calculated (**Figure S6C, D**). Within the HC alignment, two distinct clusters can be seen containing
246 the anti-capsular mAbs using to the *IGHV3-23*04*;*IGHJ4*02* combination. Interestingly, these

247 two groups contained other mAbs using the *IGHV3-23*04* or *IGHV3-21*01* V gene, suggesting an
248 association of these two V genes with anti-capsular functionality. In the LC alignment there did
249 not seem to be such a polarization, probably due to the more variegate LC recombination.
250 Nonetheless, some functional preferences could be observed, with the LC V gene *IGKV1-17*01*
251 and *IGKV1-27*01* being the most frequent anti-capsular combinations. The outcomes of these
252 analyses agreed with previously described functional clustering, reinforcing the connection
253 between sequence variations and functional attributes of the antibodies.
254

255 ## Functional profiling reveals that isolated mAbs have extremely potent bactericidal activity,
256 however only anti-capsular mAbs are poly-functional

257 To better assess protective properties of anti-capsule and anti-O-antigen bactericidal antibodies,
258 several *in vitro* assays that could predict antibody-mediated protection *in vivo* were employed.
259 Bactericidal mAbs were expressed as human IgG1 with the E430G mutation in the Fc domain,
260 which enhances the hexamerization process that naturally occurs between Fc domains and thus
261 potentiates antibody effector function[50]. The processivity of complement-dependent killing
262 assays (SBA) was enhanced by optimizing a fluorescence-based SBA (F-SBA) in the 384-well
263 format and by using resazurin metabolism as a readout of bacterial viability. F-SBA profiling of
264 mAbs against complement-sensitive pathogenic Kp strains ($ST147_{NDM-1}$, $ST147_{NDM-9}$, and
265 $ST307_{NDM-5}$) revealed that most of the antibodies were functional in the picomolar range of
266 concentrations, with the most potent mAb (05D08) showing about 0.5 ng/mL IC_{50} values (**Figure
267 4A; Figure S7A, B, C and D**). The ability to kill different Kp strains correlated with mAbs cross-
268 binding properties showed in Figure 2A, since anti-KL64 mAbs (cluster 1) were effective against
269 KL64-bearing $ST147_{NDM-1}$ and $ST147_{NDM-9}$, while anti-O-antigen mAbs (cluster 2) displayed activity
270 against O2 O-antigen-bearing $ST147_{NDM-1}$ and $ST307_{NDM-5}$ (**Figure 4A**). F-SBA results allowed
271 ranking mAbs according to their IC_{50} values and the extent of bacterial viability reduction (**Figure
272 S7E**).
273 Since phagocytes play a crucial role in Kp clearance during infection, mAbs displaying the highest
274 bactericidal potency were then evaluated in macrophage-mediated opsonophagocytosis assays.
275 Superfolder (sf) mCherry-overexpressing recombinant $ST147_{NDM-1}$ was opsonized with escalating

276 doses of mAbs prior the incubation with differentiated THP-1 cells. Then, fluorescence of
277 internalized Kp was measured as a readout of mAb ability to promote opsonophagocytosis. Anti-
278 KL64 mAbs were found to significantly increase Kp uptake by THP-1 cells at doses greater than
279 0.6 μg/mL, except for 10H18 which showed a very mild effect (**Figure 4B**). However, no significant
280 Kp uptake was detected in the presence of anti-O-antigen mAbs at none of the tested doses
281 (**Figure 4C**).
282 Finally, to analyze the impact of bactericidal mAbs on Kp cultures over time, time-lapse imaging
283 of $ST147_{NDM-1}$-sfmCherry incubated with increasing doses of mAbs was performed. Cluster 1
284 mAbs induced enchained bacterial growth in the 10 to 100 μg/mL range of concentrations (**Figure**
285 **4D**). Mechanistically, this phenotype was associated with the appearance of concatenated
286 replicating bacteria which failed to generate separate sister cells (**Supplementary Video 1**). On
287 the contrary, cluster 2 mAbs did not induce enchained growth at any tested dose (**Figure 4D;**
288 **Supplementary Video 2**).
289 Overall, this multi-functional analysis indicated that isolated mAbs had an extremely potent
290 bactericidal activity and that their functionality extended beyond opsonophagocytosis and
291 implicated other effector mechanisms, such as enchained Kp growth. However, surprisingly, only
292 anti-capsular mAbs were endowed with such poly-functionality.
293

294 ## mAb poly-functionality is required for protection against fulminant $ST147_{NDM-1}$ bloodstream
295 infection *in vivo*

296 To address the fundamental question of whether picomolar bactericidal activity on its own
297 correlates with mAb efficacy *in vivo*, or whether poly-functionality is required, the protective
298 properties of the most potent mAb candidates (anti-capsular 08O09, and anti O-antigen 05D08
299 and 05N02) were evaluated in prophylaxis (PRO) and treatment (TRT) studies in an
300 immunocompetent murine septicemia model[51]. A fulminant bloodstream infection model was
301 selected to reflect the clinical history of donors from whom mAbs were isolated and was
302 established to achieve ≥ 90% mortality within 24 hours of bacterial challenge in absence of
303 therapy (**Figure 5A**). A relatively high bacterial inoculum ($10^{6.5}$ CFU/mL) was selected to better
304 mimic the disease severity in a clinical setting.

305 To assess the *in vivo* PRO activity against $ST147_{NDM-1}$, mice were administered with 1, 5, 10, and
306 20 mg/kg mAb dose 24 hours prior to bacterial inoculation (**Figure 5B**). 08O09 PRO administration
307 at all four examined doses prolonged survival compared with sham control, with 5 mg/kg and
308 higher doses showing comparable survivals (**Figure 5C**). Instead, 05D08 and 05N02 mAbs did not
309 prolong animal survival, at none of the administered doses (**Figure 5D and E**). Consistent with
310 this observation, CFU counts in the spleen showed a reduction upon treatment with 08O09
311 (mean reduction of 1.9 to 3 $\log_{10}$ CFU) but did not show reduction in case of 05D08 and 05N02
312 (**Figure 5F**). PRO experiment with 5 mg/kg 08O09 dose was repeated on 30 animals in total in
313 three separate experiments, showing consistency and reproducibility, with approximately 50%
314 survival up to 96 hours (**Figure 5G**). Plasma concentration of 08O09 associated with *in vivo*
315 efficacy amounted to 74.3 ± 21.7 µg/mL (**Figure 5H**). Hence, consistent survival results and
316 decrease in organ bacterial load using 08O09 5 mg/kg PRO across runs demonstrated the
317 robustness of the model to delineate efficacy *in vivo*.
318 Considering these results, the treatment (THR) efficacy of 08O09 administered intravenously at
319 1, 5, 10, and 20 mg/kg one-hour post-bacterial challenge was assessed **(Figure 6A)**. In this case,
320 08O09 THR at the four examined doses resulted in significantly prolonged survival compared with
321 sham control **(Figure 6B)**, which was associated with 1 to 2.4 mean $\log_{10}$ CFU reduction in the
322 spleen **(Figure 6C)**. Survival was comparable among groups treated with 5 mg/kg and higher
323 doses.
324 Lastly, the protective properties of 08O09 in a combined prophylaxis/treatment (PRO+THR)
325 regimen were measured. In this case, the first dose of 08O09 was administered intraperitoneally
326 24 hours before bacterial inoculation, and the second dose was administered intravenously one-
327 hour post-bacterial challenge **(Figure 6D)**. Interestingly, an advantage of using a combinatorial
328 treatment, with 30% survival till 96 h, was observed only for 1 mg/kg dosage that was otherwise
329 suboptimal in monotherapy regimens (**Figure 6E**). However, when 08O09 was administered at 5
330 mg/kg, PRO monotherapy performed significantly better than combinatorial treatment (**Figure
331 6F**), suggesting that while a suboptimal mAb dosing could be compensated by combined regimen,
332 an optimal mAb dosing may perform well as a monotherapy. Overall, these experiments

333 demonstrated that an anti-KL64-specific poly-functional mAb protects animals in PRO and THR
334 regimens by efficiently reducing the systemic load of pandrug-resistant $ST147_{NDM-1}$.
335
336

337 ## DISCUSSION

338

339 In this work, we presented a rationally designed pipeline to screen and isolate protective human
340 mAbs against hypervirulent and pandrug-resistant $ST147_{NDM-1}$ Kp. This strain, which was obtained
341 from a highly persistent nosocomial outbreak that started in 2018 in the hospital of Pisa in Italy,
342 is now endemic in the region[19–21]. Moreover, $ST147_{NDM-1}$ Kp is also spreading globally with high
343 speed and has already been described in Europe[20,52], USA[53], and Southeast Asia[54]. Our antigen-
344 agnostic approach resulted in the selection of human mAbs that can be exploited as therapeutic
345 and prophylactic agents against $ST147_{NDM-1}$. Of note, we identified *in vitro* assays that correlate
346 with protection. Through this strategy, we discovered and characterized the first human mAb
347 which interacts with capsule type KL64 and protects against fulminant bloodstream infection by
348 the pandrug-resistant Kp strain.

349 Our data highlight the importance of developing robust predictive assays to correlate *in vitro*
350 mAb functionality with *in vivo* efficacy. Out of more than 200 $ST147_{NDM1}$-specific mAbs isolated
351 from convalescent donors, we found 20 highly bactericidal antibodies targeting either the
352 capsule or the O-antigen, all working in the picomolar range of concentrations. However, despite
353 the similar potency in the bactericidal assay, only a subset of them promoted phagocytosis and
354 bacterial enchained growth, which correlated with protection against bloodstream infection. This
355 evidence indicated that bactericidal activity, which is usually a strong correlate of protection, is
356 not sufficient for *in vitro* mAbs characterization and identification of the best candidate, whereas
357 *in vitro* poly-functionality is an essential feature that protective mAbs must bear, particularly in
358 the case of those targeting the pandrug-resistant strain $ST147_{NDM-1}$. Lack of correlation with
359 complement-mediated bactericidal activity and the positive correlation with phagocytosis are
360 aligned with the knowledge that Kp killing and clearance is impaired when cellular innate immune
361 functionality is decreased or deficient[55,56]. In particular, increased susceptibility to Kp infections
362 has been observed in association with neutrophil deficiencies[56,57].

363 Noteworthy, the capsule is an important virulence factor for Kp pathogenesis which shields
364 bacteria against the host immune response[58–61]. Previous studies showed that mutations
365 preventing capsule synthesis transformed Kp strains into avirulent bacteria when infecting rats

366 or mice[59,62,63]. Likewise, it has been reported that in some cases anti-O-antigen mAbs were
367 protective only against non-encapsulated Kp strains[64], suggesting that Kp capsule is an important
368 immune evasion factor. Although we did not explore this aspect in the present work, we found
369 that O-antigen-specific mAbs were devoid of *in vitro* poly-functionality and *in vivo* efficacy,
370 implying that KL64 capsule might limit their access to the cognate epitopes thereby interfering
371 with their action. Another possibility that has remained unexplored is that, during *in vivo*
372 infection, KL64 capsule production could be dynamically modulated to further increase the
373 shielding effect. Hence, KL64 capsule represents a strategically important immunodominant
374 antigen to be neutralized.
375 By correlating *in vitro* and *in vivo* results we propose that anti-KL64 capsule mAbs protect *in vivo*
376 by means of two main mechanisms of action, the first being macrophage-mediated killing. An
377 additional underexplored mechanism of immune protection employed by KL64-targeting mAbs
378 is triggering bacterial enchained growth *in vitro*. Bacterial concatenation induced by secretory
379 dimeric IgA (sIgA) has been previously described as a protective mechanism restricting
380 *Salmonella* Typhimurium growth and facilitating its clearance from the intestine[65,66].
381 Interestingly, here we observed that this phenomenon applies to Kp as well and can be promoted
382 by monomeric IgG. Moreover, considering that only anti-capsule and not anti-O-antigen mAbs
383 induce enchained growth, we ought to think that targeting the most external bacterial layer (*i.e.*
384 the capsule) is essential to promote enchainment.
385 $ST147_{NDM-1}$ has been classified as a pandrug-resistant and hypervirulent strain[26] which has not
386 only been responsible for local outbreaks in Italy[19–21] but has been causative of infections
387 worldwide[20,52–54]. Additionally, genomic surveillance reports indicate that KL64, associated with
388 enhanced virulence[67], is replacing some previously prevalent capsular loci through intraspecies
389 clone shifting[68] and became the third emerging capsule type for hypervirulent strains after K1
390 and K2 serotypes[4,69]. Indeed, carbapenem-resistant KL64-expressing ST11 Kp represents the
391 most common AMR lineage in China[70]. Taken together, these data underline the importance of
392 anti-capsular mAbs to contain and prevent future outbreaks caused by $ST147_{NDM-1}$ and other
393 KL64-bearing Kp isolates. As such, 08O09 mAb, developed in the pursuit of an effective therapy

394 against a regional outbreak of a pandrug-resistant strain, might represent an excellent candidate
395 for treatment and prophylaxis of KL64 Kp infections globally.
396

397 ## LIMITATIONS OF THE STUDY

398 Hyper-capsulation of $ST147_{NDM-1}$ Kp may explain why, despite applying an antigen-agnostic
399 approach, we pinpointed only anti-capsule and anti-OAg bactericidal mAbs, while no bactericidal
400 antibodies against other type of antigens were identified. Indeed, Kp protein antigens may be
401 masked by the thick OAg and capsule layers, which probably elicited most of the humoral
402 immune response with bactericidal activity. While the work resulted in the identification of a
403 candidate effective medication against $ST147_{NDM-1}$ Kp, clinical application of 08O09 to Kp
404 infections will be limited to the KL64 serotype. In the framework of exploiting mAbs for anti-Kp
405 universal vaccine design, future research efforts should be directed towards the identification of
406 functional antibodies against conserved targets. To this end, implementation of specific
407 screening strategies will be instrumental. Finally, careful choice of the target patients who may
408 benefit from mAb-based therapy should be made since $ST147_{NDM-1}$ Kp can cause acute infections
409 as well as chronic colonization which may require differential treatment protocols.
410

411 ## ACKNOWLEDGMENTS

412 We wish to thank all patients who participated in this study. We acknowledge Federica Romano,
413 Giulia Fantoni, Giulio Pierleoni and the Clinical Studies team at Fondazione Toscana Life Sciences
414 for technical support and help with clinical study documentation; Valentina Galfo (University of
415 Pisa) for the contribution to patient sampling and enrolment; Simona Tavarini and Chiara
416 Sammicheli (GlaxoSmithKline, Siena, Italy) for help with cell sorting and flow cytometry; Maria
417 Grazia Pizza (Imperial College, London, UK) for insightful discussion; Francesca Micoli, Carlo
418 Giannelli, Omar Rossi, Gianmarco Gasperini (GlaxoSmithKline, Siena, Italy) for technical advice on
419 Klebsiella antigen purification; Chris Whitfield and Steven Kelly (Department of Molecular and
420 Cellular Biology, University of Guelph, Guelph, Ontario, Canada) for the generous gift of Kp LPS;
421 Maria Grazia Cusi (University Hospital of Siena), Deborah Hung (The Broad Institute of MIT and
422 Harvard, Cambridge, MA, USA), Joshua Liang Chao L.C. Wong and Gad Frankel (Department of

Life Sciences, MRC Centre for Molecular Bacteriology and Infection, Imperial College London, London, UK) for providing Kp strains and insightful discussion.

AUTHOR CONTRIBUTIONS

Conceptualization: CS, AK, RR; methodology: ER, VZGF, SSB, IP, GM, AK; investigation: ER, VZGF, SSB, IP, GM, GB, SS, GC, SY, LC, MR, MT, NM, CM, CDS, AC, LC, ; bioinformatic analysis: GM, DC; resources: GT, CG, LC, SB, FM, MF, DPN, KA; data curation: GM, DC, MF, DL; writing – original draft: ER, VZGF, SSB, GM, GB; writing – review & editing: ER, VZGF, SSB, GM, DPN, KA, CS, AK, RR; visualization: ER, VZGF, SSB, GM, AK; supervision and funding acquisition: CS, AK, RR.

FUNDING

This project was supported by funds of the Centro Regionale per la Medicina di Precisione (CREMEP) and by PROREACT (progetto finanziato con le risorse del Fondo per il rilancio degli investimenti delle amministrazioni centrali dello Stato e allo sviluppo del Paese, di cui all'art. 1 comma 95, n. 145/2018, fondi 2019-2023, del Ministero della Salute).

DECLARATION OF INTERESTS

Patent application 102023000000924 describing isolated mAbs has been filed by Fondazione Toscana Life Sciences.

R.R. hold shares in the GSK group of companies and declare no other financial and non-financial relationships and activities. Remaining authors declare no competing interests.

445 FIGURE LEGENDS

446

447 **Figure 1. Isolation and selection of Kp-specific mAbs against ST147$_{NDM-1}$ Tuscany outbreak**
448 **strains.** (A) Schematic workflow of anti-Kp antibody isolation and selection. (B) ELISA screening
449 of supernatants of 18,390 single cell-sorted MBCs isolated from 7 convalescent patients. The
450 assay was performed to detect IgG/IgA against surface antigens of ST147$_{NDM-1}$ c.i.1 and ST147$_{NDM-}$
451 $_{1}$ c.i.2. 214 MBCs supernatants showed a signal at least 2-fold above the blank of OD_{405} and were
452 thus selected for further analysis (blue dots). (C) L-SBA on recombinant mAbs against ST147$_{NDM-1}$
453 c.i.1. 30% reduction in bacterial viability was used as a cut-off for selection. 25 mAbs showing
454 bactericidal properties were identified (red dots).

455

456 **Figure 2. Binding properties of 20 bactericidal ST147$_{NDM-1}$-specific mAbs.** (A) Heatmap showing
457 high-throughput flow cytometry screening of 20 functional mAbs against a panel of genetically
458 diverse Kp strains. MFI was normalized to no mAb controls and transformed in logarithmic scale.
459 (B) Heatmap of ELISA values obtained with 08O09 (cluster 1 mAb) and cluster 2 mAbs against
460 ST147$_{NDM-1}$ c.i.1, ST147$_{NDM-9}$ (wt), ST147$_{NDM-9}$/pSEVA23a1_*wbbO* (*wbbO*$^{+}$), ST147$_{NDM-}$
461 $_{9}$/pSEVA23a1 (*wbbO*$^{-}$) strains. (C-E) Immunoblot (IB) of 05N02 (panel C), 05D08 (panel D) and
462 08O09 (panel E) against ST147$_{NDM-1}$ c.i.1, ST147$_{NDM-9}$ (wt), ST147$_{NDM-9}$/pSEVA23a1_*wbbO*
463 (*wbbO*$^{+}$), ST147$_{NDM-9}$/pSEVA23a1 (*wbbO*$^{-}$) strains. (F) Heatmap of ELISA with purified capsule and
464 O-antigens. Unrelated *E. coli* LPS O111:B4 was used as negative control and total bacterial lysate
465 as a positive control. Values at least 3-fold above the blank of OD_{405} were considered as positive
466 hits. (G-I) Representative immunoblots (IB) of selected anti-Kp mAbs probed against total sugar
467 extracts of indicated strains. 08O09 (panel G) recognizes high molecular weight KL64 capsule.
468 05N02 (panel H) recognizes O-antigens with broad molecular weight distribution belonging to
469 O2- and O1 types. 05D08 (panel I) recognizes medium molecular weight O-antigen structures
470 from O2-carrying Kp strains.

471

472 **Figure 3. Microscopy characterization of anti-Kp mAb binding on ST147$_{NDM1}$ c.i. 1 strain.** (A)
473 Images show ST147 $_{NDM-1}$ c.i. 1 expressing sfmCherry stained with 08O09, 05D08 and 05N02 mAbs

474 labelled with anti-human A488 conjugated secondary antibody (green). Bacterial DNA is stained
475 with DAPI (blue). Scale bar 2 µm. (B) Scatter plot showing quartiles range of A488 intensity
476 quantification at the single bacterium level (median intensity ± sd/number of bacteria are
477 reported for each mAb: 12289±9278 a.u./3475 for 08O09; 2518±1250 a.u./3024 for 05D08;
478 2860±1601 a.u./3269 for 05N02; 119.1±3.7 a.u./3078 for unrelated mAb). Two-way ANOVA from
479 4 independent experiments, * p=0.0143; **** p<0.0001. (C) Scatter plot displaying quartiles
480 range of the area of individual A488 spots (median area ± sd/number of spots are reported for
481 each mAb: 8.3±3.4 μm^2/3475 for 08O09; 4.9±1.6 μm^2/3072 for 05D08; 4.8±1.5μm^2/3310 for
482 05N02). Two-way ANOVA from 4 independent experiments, **** p<0.0001; ns, non-significant.
483 (D) Images of $ST147_{NDM1}$ c.i. 1 stained with 08O09-A488 (green), 05N02-A555 (yellow) conjugated
484 mAbs and DAPI (blue). Scale bar 2 µm. (E) Representative images showing $ST147_{NDM1}$ c.i. 1 stained
485 with 08O09-A488 (green), 05N02-A555 (yellow) and 05D08-A647 (red) conjugated mAbs. DNA
486 was stained with DAPI (blue). Scale bar 2 µm.
487
488 **Figure 4. Functional *in vitro* characterization of bactericidal $ST147_{NDM-1}$-targeting mAbs.** (A)
489 Heatmap reporting mean IC_{50} values resulting from F-SBA screening of 20 anti-Kp mAbs against
490 the indicated Kp strains. Values for each mAb result from 2 to 6 replicated experiments. (B)
491 Bacterial fold uptake by THP-1 macrophages measured in phagocytosis assay in the presence of
492 anti-Kp mAbs from cluster 1 on $ST147_{NDM1}$ c.i. 1-sfmCherry. Two-way ANOVA test to compare
493 each anti-Kp mAb to the unrelated mAb resulted in the following *P* values at the minimum
494 effective dose: p=0.0004 and p=0.001 for 03F18 and 08O09, respectively, at 0.625 µg/mL;
495 p=0.016 for 08D18 at 1.25 µg/mL; p=0.004 and p=0.035 for 08K19 and 10H18, respectively, at 2.5
496 µg/mL. Experimental replicates: N=6 for 03F18; N=4 for 08O09; N=5 for 08D18; N=4 for 08K19;
497 N=6 for 10H18. (C) Bacterial fold uptake by THP-1 cells measured in samples treated with anti-Kp
498 mAbs from cluster 2 on $ST147_{NDM1}$ c.i. 1-sfmCherry. Two-way ANOVA test to compare each anti-
499 Kp mAb to the unrelated mAb resulted in no significant *P* values at any tested dose. Experimental
500 replicates: N=2 for 05D08 and 05N02; N=3 for 05M13. (D) Panels show still frames from time-
501 lapse imaging of on $ST147_{NDM1}$ c.i. 1 bacteria expressing sfmCherry and incubated with 100 µg/mL
502 of indicated mAbs for 120 min. Scale bar 5 µm.

503

504 **Figure 5. Evaluation of *in vivo* prophylactic efficacy of 08O09, 05D08 and 05N02 mAbs in**
505 **immunocompetent ST147$_{NDM-1}$ bacteremia model.** (A) Survival analysis for groups of mice
506 infected with ST147$_{NDM-1}$ c.i. 1 at four tested inoculums (n=10 animals per group). (B) Scheme of
507 the prophylaxis (PRO) study. (C-D) Survival analysis of 08O09 (C), 05N02 (D) and 05D08 (E) PRO
508 regimens versus sham controls (n=10 mice per group). Indicated *P* value was calculated by log-
509 rank test and refers to a comparison of every 08O09-treated group versus the control group for
510 each indicated administration dose. (F) Spleen load of ST147$_{NDM1}$ in 08O09 PRO study. Log$_{10}$
511 CFU/spleen at endpoint (n=10 animals per group) was normalized to non-infected controls (n=6
512 animals). Indicated are mean values; Mann-Whitney test * p< 0.05, ** p< 0.01, *** p<0.001, ****
513 p<0.0001. (G) Survival analysis of 08O09 PRO regimens administered as a single dose of 5 mg/kg
514 in three independent experiments versus sham controls (n=10 mice per group). Log-rank test to
515 compare each 08O09-treated group versus the respective control group resulted in the following
516 *P* values: <0.0001 for study #1; 0.0049 for study #2, <0.0001 for study #3. (H) Concentration of
517 08O09 mAb in mouse plasma was measured by ELISA 24 hours after 5 mg/kg i.p. administration
518 (n=6 animals). Statistical bar indicates mean values ± SD.

519

520 **Figure 6. Evaluation of *in vivo* therapeutic and combined efficacy of 08O09, 05D08 and 05N02**
521 **mAbs in immunocompetent ST147$_{NDM-1}$ bacteremia model.** (A) Scheme of treatment (THR)
522 study. (B) Survival analysis of 08O09 THR regimens versus sham controls (n=10 mice per group).
523 Log-rank test to compare each 08O09-treated group versus the respective control group resulted
524 in the following *P* values: 0.0002 for 1 mg/kg; 0.0005 for 5 mg/kg, and <0.0001 for 10 and 20
525 mg/kg. (C) Spleen load of ST147$_{NDM1}$ in 08O09 THR study. Log$_{10}$ CFU/spleen at endpoint (n=10
526 animals per group) was normalized to non-infected controls (n=6 animals). Mann-Whitney test *
527 p< 0.05, **** p<0.0001. (D) Scheme of prophylaxis plus treatment (PRO+THR) study. (E) Survival
528 analysis of 08O09 PRO regimens and PRO+THR regimens at 1 mg/kg doses (n=10 mice per group).
529 Indicated *P* values were calculated by log-rank test and refer to a comparison of PRO+THR group
530 versus either PRO (p<0.05) or THR group (p<0.001). (F) Survival analysis of 08O09 PRO regimens

531 and PRO+THR regimens at 5 mg/kg doses (n=10 mice per group). Indicated *P* values were
532 calculated by log-rank test and refer to comparisons indicated by brackets.

533 TABLES

Table 1. List of Kp isolates used in the manuscript. ST, K locus, O locus and presence of carbapenemase gene information were predicted from genomic analysis.

Strain name	Infection type	ST	K locus	O locus	O type	Carbapenemase gene	Origin
$ST147_{NDM-1}$ c.i.1	Bacteremia	147	KL64	O2v1	O2a	bla_{NDM-1}	this study*
$ST147_{NDM-1}$ c.i.2	Bacteremia	147	KL64	O2v1	O2a	bla_{NDM-1}	this study*
$ST147_{NDM-9}$	Bacteremia	147	KL64	O2v1	O2a	bla_{NDM-9}	this study*
$ST307_{NDM-5}$	Abdominal drainage	307	KL102	O2v2	O2afg	bla_{NDM-5}	this study*
ST258	UTI	258	KL107	O2v2	O2afg	-	UCI_38 / Biosample ID SAMN02356618
$ST512_{VIM}$	n/a	512	KL107	O2v2	O2a	bla_{VIM}	this study*
$ST13_{OXA-48}$	Intestinal carriage	13	KL57	O1v2	O1	bla_{OXA-48}	this study*
ST493	n/a	493	KL2	O1v1	O1	-	ATCC43816

*BioProject PRJNA1067287

534

535

536

537

538 ## MATERIALS AND METHODS

539

540 ### Enrollment of Kp-infected patients

541 Clinical protocol Klebsiella01 was approved by the ethics committee of the University Hospital of
542 Pisa (Parere 16526). All enrolled patients signed a written informed consent form before taking
543 part in the study which was conducted in accordance with Good Clinical Practice (GCP) guidelines
544 and ethical principles of the Declaration of Helsinki. Patients' information can be found in Table
545 S1.

546

547 ### Bacterial strains and culture conditions

548 Bacterial strains used in this work are listed in Table 1. Kp isolates were grown at 37°C in LB broth
549 in the presence of the appropriate antibiotic (5 µg/mL meropenem for $ST147_{NDM-1}$ c.i.1, $ST147_{NDM-}$
550 $_{1}$ c.i.2, $ST147_{NDM-9}$,$ST307_{NDM-5}$, $ST13_{OXA-48}$, $ST512_{VIM}$; 150 µg/mL hygromycin for sfmCherry
551 $ST147_{NDM-1}$ c.i. 1), or on LB-agar plates supplemented with the appropriate antibiotic (5 µg/mL
552 meropenem for $ST147_{NDM-1}$ c.i.1, $ST147_{NDM-1}$ c.i.2, $ST147_{NDM-9}$,$ST307_{NDM-5}$, $ST13_{OXA-48}$, $ST512_{VIM}$;
553 150 µg/mL hygromycin for sfmCherry $ST147_{NDM-1}$ c.i. 1). All other bacterial strains were grown in
554 LB.

555

556 ### Single-cell sorting of memory B cells from convalescent donors

557 Peripheral blood mononuclear cells (PBMCs) were isolated from heparin-treated whole blood by
558 density gradient centrifugation (Ficoll-Paque PREMIUM, GE Healthcare). After separation, PBMC
559 were stained with Live/Dead FSV780(BD Horizon) in 100 µL final volume diluted 1:1000 at room
560 temperature (RT). After 20 min of incubation, cells were washed with phosphate-buffered saline
561 1X (PBS) and unspecific bindings were saturated with 50 µL of 20% normal rabbit serum (Life
562 Technologies) in PBS. Following incubation at 4°C for 30 min, cells were washed with PBS 1X,
563 centrifuged at 1200 rpm for 8 min, and stained with CD19 APC (BD cat# 561742), IgM PeCF594
564 (BD cat# 562539), CD27 APCR700 (BD cat# 565116), IgD PE (BD cat# 562024), CD3 PE-Cy7 (BD
565 cat# 560910), CD14 PE-Cy7 (BD cat# 560919) and CD56 PECy7 (BD cat# 560916) in Staining Buffer
566 (1% Fetal Bovine Serum in PBS) at 4°C for 30 min. Following additional washing, cells were
567 resuspended in Sorting Buffer (PBS/EDTA 2.5 mM). Stained memory B cells (MBCs;

568 CD3/CD14/CD56$^-$ CD19$^+$ CD27$^+$ IgD$^-$ IgM$^-$) were single-cell sorted with a BD FACSAria™ Fusion (BD
569 Biosciences) into 384-well microplates containing 3T3-CD40L feeder cells and were incubated
570 with IL-2 and IL-21 for 14 days[71].
571

572 ## ELISA screening of mAb binding against *Klebsiella pneumoniae*

573 Supernatants resulting from single-cell sorting of MBCs were used as a source of IgG1 and IgA
574 monoclonal antibodies (mAbs) to test their binding to whole bacteria in a high-throughput
575 enzyme-linked immunosorbent assay (ELISA). Pools of ST147$_{NDM-1}$ c.i. 1 and ST147$_{NDM-1}$ c.i. 2
576 (**Table 1**) were grown in LB medium, pelleted at exponential phase (OD_{600}=0.5), resuspended in
577 PBS, and plated into 384-well plastic plates (Greiner, ref. 781101). Plated bacteria were fixed at
578 RT for 30 min in 0.5 % of paraformaldehyde. Plates were then blocked in PBS plus 2% Calf Serum
579 (Euroclone, ECS0040L) at RT for 1 h. After incubation, bacteria were incubated for 1 h with MBC
580 supernatants diluted in PBS plus 2% Calf Serum. Next, anti-human IgG and anti-human IgA
581 secondary antibodies conjugated with Alkaline Phosphatase (Southern Biotech) were added for
582 45 min. To detect bacteria-mAbs binding, pNPP (p-nitrophenyl phosphate; Sigma-Aldrich) was
583 used as soluble substrate and the final reaction was quantified at a wavelength of 405 nm by
584 using the Varioskan Lux Reader (Thermo Fisher Scientific). After each incubation step, plates
585 were washed three times with 100 µl per well of washing buffer (PBS and 0.05% Tween-20).
586 Sample buffer was used as a blank and we considered as positive hits those wells showing an
587 OD_{405} value of at least 2-fold superior to blank. Cells corresponding to positive hits were lysed in
588 25 µL of a buffer containing RNAse Out 0.2 U/µL, ultrapure BSA 1 mg/mL and DEPC H_2O (Thermo
589 Fisher Scientific) and stored at -80°C until use.
590

591 ## Single-cell RT-PCR and nested PCR were used to amplify V_H and V_L

592 cDNA was synthesized from 5 µL of MBC lysates. Reverse transcription (RT) reaction was
593 performed by adding 25 µL per well of a mix containing 1 µL of random hexamer primers (50
594 ng/mL),1 µL of dNTPs (10 mM), 2 µL 0.1 M DTT, 40 U/µL Rnase OUT, $MgCl_2$ (25 mM), 5 µL of 5X
595 buffer, 0.25 µL of Superscript IV reverse transcriptase (Invitrogen) and nuclease-free water
596 (DEPC) and RT-PCR conditions were 42°C/10 min, 25°C/10 min, 50°C/ 60 min and 94°C/5 min.

597 After cDNA synthesis, two additional rounds of PCR were performed to obtain the variable
598 regions of the heavy (V_H) and light (V_L) chains. Briefly, in the first round of PCR (PCR I) a total
599 volume of 25 µL containing 4 µL of cDNA, 10 µM of VH or 10 µM VL/VK primer mix (**Table S2**),
600 0.5 µL of dNTPs (10 mM), 1.5 µL $MgCl_2$ (25 mM), 5 µL of 5X Kapa Long Range Buffer, and 0.125
601 µL of Kapa Long Range Polymerase (Sigma) was added in each well and amplified using the
602 following conditions: 95°C/3', 5 cycles at 95°C/30'', 57°C/30'', 72°C/ 30'' and 30 cycles at
603 95°C/30'', 60°C/30'', 72°C/30'' and 72°C/2'. 3 µL of un-purified PCR I products were used as a
604 template for the nested PCR (PCR II) using the same cycling conditions and primers indicated in
605 **Table S2**. PCR II products were then purified by Millipore MultiScreen PCR 96 plate according to
606 the manufacturer's instructions. Samples were eluted in 30 µL nuclease-free water pre-warmed
607 at 50°C and quantified by NanoDrop One (Thermo Fisher Scientific).
608

609 ### Cloning of V_H and V_L and recombinant antibody expression by TAP transfection

610 Amplified antibody sequences were ligated into human IgG1 expression vectors and used to
611 produce transcriptionally active PCR (TAP) products. Briefly, IgG1, Igκ or Igλ expression vectors
612 were digested with AgeI, SalI and XhoI restriction enzymes, respectively. 25 ng of linearised
613 plasmids were ligated with 75 ng of purified V_H and V_L by Gibson Assembly (New England
614 BioLabs). The reaction was performed in a final volume of 5 µL. The ligation product was 10-fold
615 diluted in DEPC water and used as a template for transcriptionally active PCR (TAP) reaction
616 which allowed the direct use of linear DNA fragments for *in vitro* expression. Functional promoter
617 (human CMV) and terminator sequences (SV40) were attached onto PCR II products directly by
618 amplification using specific primers (**Table S2**). TAP-PCR was performed in a total volume of 25
619 µL containing 0.25 µL of Q5 polymerase (NEB), 5 µL of GC Enhancer (NEB), 5 µL of 5X buffer, 0.5
620 µL dNTPs (10 mM), 0.125 µL of forward/reverse primers and 3 µL of ligation product, and using
621 the following conditions: one step of 98°C/2', 35 cycles of 98°C/10'', 61°C/20'', 72°C/1' and an
622 extension of 72°C/5'. Once purified and quantified, TAP products were transfected into Expi293F
623 cells to allow small scale production of recombinant mAbs. Briefly, cells were transfected with
624 both TAP amplifications in a final volume of 1 ml into 96 deep well plate (Eppendorf), and after
625 7 days of expression mAb-containing supernatants were harvested by centrifugation.

626

627 ## Quantification of TAP-produced mAbs by ELISA

628 To quantify the concentration of mAbs in each supernatant, ELISA plates were coated with 2
629 µg/ml of goat anti-human IgG (Southern Biotech) at 4°C overnight. Plates were washed 3 times
630 with PBS plus Tween-20 0.05 %, blocked in PBS plus BSA 1% at 37°C for 1 h. Then samples were
631 washed and incubated with TAP-produced mAbs diluted in sample buffer (PBS – BSA 1 %- Tween-
632 20 0.05%) at 37°C for 1 h. Following additional washings and incubation at 37°C for 1 h with AP-
633 conjugated anti-goat IgG secondary antibody (Southern Biotech), absorbance was read by
634 addition of PNPP. Concentrations were evaluated by linear regression analysis built by potting
635 OD_{405} values against a standard curve generated by titration of a human IgG-unlabeled antibody
636 (Southern Biotech).

637

638 ## Large scale expression and purification of mAbs

639 Expi293F cells (Thermo Fisher) were transiently transfected with plasmids carrying the heavy and
640 the light chains of each antibody with a 1:2 weight/weight ratio. Cells were grown for six days at
641 37°C with 8% CO_2 and 125 rpm shaking, with an optimized cocktail of enhancers 1 and 2 (Thermo
642 Fisher) added on day 1 post-transfection. Two mAb harvests were performed on the third and
643 sixth day by pelleting the cells at 1,100 x g for 10 min at RT and supernatants were pooled and
644 clarified by centrifugation (3,000 x g for 15 min at 4°C), followed by 0.45 mm filtration. mAbs
645 were purified at RT by affinity chromatography on the AKTAgo purification system (Cytiva) using
646 the HiTrap Protein G HP column (Cytiva), which binds to the Fc domain. Specifically, the column
647 was equilibrated in 0.02 M sodium phosphate buffer pH 7 at a flow rate of 1 mL/min, which was
648 used also for the following steps. After sample injection, the column was washed with 10 column
649 volumes (CV), followed by mAb elution with 10 CV of 0.1 M glycine-HCl, pH 2.7. mAb pool was
650 dialyzed in PBS pH 7.4 using Slide-A-Lyzer G2 Dialysis Cassette 3.5K (Thermo Scientific) overnight
651 at 4°C. For each purified antibody, the concentration was determined by measuring absorbance
652 at 280 nm by Nanodrop. All purified antibodies were aliquoted and stored at -80°C.

653

654 ## Serum Bactericidal Assay (SBA)

655 Two days prior to the assay, glycerol stocks of Kp were streaked on LB-Agar plates and incubated
656 overnight (ON) at 37°C. On the following day, a single colony was inoculated in 4 mL of LB and
657 incubated ON at 37°C. Cultures were expanded to 10 mL LB in a 125 mL flask to obtain an OD_{600}
658 of 0.05 and incubated at 37°C with shaking until the exponential phase (OD_{600} 0.4-0.6) was
659 reached. Bacteria were then 1:10 diluted in PBS.

660 Appropriate baby rabbit complement (BRC, Cedarlane) concentrations to be used in the assay
661 were established through complement sensitivity tests. Briefly, $2x10^5$ bacteria resuspended in
662 PBS were seeded in round bottom 96-well plates, and BRC concentrations were screened starting
663 from 50% in 11 serial 2-fold step dilutions. After 2 h incubation at 37°C, bacteria were pelleted
664 by centrifugation. The supernatant was discarded, and bacteria were resuspended in 30 µl of PBS
665 and transferred into a White Optiplate (Perkin Elmer). 30 µl of BacTiter-Glo™ 1X (Promega) was
666 added to each well and luminescence was measured by the Varioskan Lux microplate reader
667 (Thermo Fisher Scientific) with an exposure time of 500 ms. Data were plotted and analysed using
668 GraphPad Prism. 12.5 % BRC was chosen as the BRC concentration allowing to achieve
669 complement-based antibody killing without significant toxicity.

670 For luminescence-based SBA (L-SBA) with TAP-expressed mAbs, $2x10^6$ bacteria/mL of $ST147_{NDM-}$
671 $_{1}$ were seeded into a 96-well U-round bottom plate in the presence of 12.5% BRC, with the
672 addition of four serial dilutions of TAP-expressed mAbs (1:10, 1:50: 1:250: 1:1250), in a total
673 volume of 100 µl per well. Upon 2 h incubation at 37°C, bacteria were pelleted by centrifugation
674 at 4000 xg. Bacterial pellets were resuspended in 30 µl of PBS per well and transferred into a
675 white Optiplate (Perkin Elmer). 30 µl of BacTiter-Glo™ 1X (Promega) was added to each well and
676 luminescence was measured by the Varioskan Lux microplate reader (Thermo Fisher Scientific)
677 with 500 ms exposure. In each experiment, luminescence values obtained were used to calculate
678 the median value for each dilution factor. The difference between the luminescence signal of
679 each mAb and the median value was measured and plotted as percentage with 30 % cut-off.

680 For fluorescence-based SBA (F-SBA), $2x10^6$ bacteria/mL in PBS were seeded in 384-well black
681 clear-bottom plate (ViewPlate®-384 F TC, PerkinElmer) in the presence of 12.5 % BRC, in a final
682 volume of 50 µl per well. Purified recombinant mAbs were added in a 3-fold step serial dilution

683 panel. After 2 h incubation at 37°C, 40 µl LB and 10 µl of 0.025% resazurin (Sigma-Aldrich) were
684 added to each well. Fluorescence (λ_{Ex} 560 nm and λ_{Em} 590 nm, exposure: 250 ms) was measured
685 by the Varioskan Lux microplate reader (Thermo Fisher Scientific) upon 2 h incubation at 37°C.
686 GraphPad Prism was used to plot and analyse data, as well as to extrapolate IC_{50} values.
687

688 ### Flow cytometry analysis of mAb binding to bacterial surface

689 Binding of mAbs to the bacterial strains listed in Table 1 was assessed in the exponential phase
690 of growth in LB (OD_{600} 0.4-0.6). Bacteria were pelleted and resuspended in an equal volume of
691 PBS- BSA 1%. 100 µL of bacteria were plated in each well of a round bottom 96-well plates by
692 centrifuging at 4000 x g for 5 min, followed by incubation with 5 µg/ml of purified antibodies at
693 RT for 1 h. Plates were centrifuged, and pellets were washed three times with PBS – BSA 1% and
694 incubated at RT for 30 min in the dark with 1:2000 diluted Alexa488-conjugated α-human IgG
695 secondary antibody. After an additional centrifugation and washing step, bacteria were fixed
696 with 0.5% of paraformaldehyde at RT for 30 min, washed again, resuspended in PBS – BSA 1% to
697 an OD_{600} of 0.05 and read by their fluorescence. Samples were acquired on the BD FACS Canto II
698 (BD Biosciences, USA). Data were analysed by FlowJo software v10 (BD Biosciences, USA).
699

700 ### Antibody sequence analysis

701 Immunoglobulin genes were identified with NCBI IgBlast[72] and named according to the IMGT
702 nomenclature (in the time between 2020 and 2022). IGHV gene somatic hypermutations were
703 counted from the start of FWR1 until the end of FWR3. Insertions or deletions were counted as
704 one single mutation.
705

706 ### Genomic analysis of Kp isolates

707 ST147 strains were sequenced using both short- and long-reads technology. High-throughput-
708 sequencing was performed on the MiSeq platform (Illumina; San Diego, CA, USA) with a paired-
709 end layout of 150 bp. Paired-end short reads were quality-checked and poor-quality reads were
710 filtered using fastp v0.20.1[73]. The long-read library was prepared with multiplexing and
711 sequenced according to the manufactures' guide using flow cell R9.4.1 (Nanopore). The quality

712 of long reads was controlled by being mapped with their corresponding short reads using Filtlong
713 v0.2.0 (https://github.com/rrwick/Filtlong) with minimum quality and length as Q8 and 2,000 bp
714 respectively. Along with the corresponding clean reads, long reads were fed into the hybrid
715 assembler Unicycler v0.4.8[74] and run under the conservative mode. ST and capsule typing
716 prediction was performed using Kleborate v2.0.0[10] and Kaptive[75]. Roary[76] version 3.13.0 was
717 used for pan-genome analysis, and the core gene alignment from Roary was used to generate a
718 core gene single nucleotide polymorphism (SNP) tree. First, SNP sites in the core gene alignment
719 from Roary were concatenated with snp-sites[77] version 2.4.1. The resulting concatenated SNPs
720 were used in IQ-Tree[78] version 1.6.8 to create a maximum likelihood (ML) tree. The optimal
721 evolutionary model was selected by using ModelFinder plus. Raw sequencing data have been
722 released under BioProject PRJNA1067287.
723

724 ### Immunoblot analysis of mAb binding to Kp lysates

725 For sample preparation, bacteria from glycerol stocks were grown overnight on LB-agar plates.
726 Single colonies of Kp were picked from plates and grown overnight with static incubation at 37°C
727 in LB. On the following day, bacteria were grown at 37°C starting from OD_{600} 0.05 with shaking
728 in LB until they reached the exponential phase (OD_{600} 0.4-0.6). Polysaccharide extracts were
729 prepared by phenol extraction. Following overnight growth, bacteria were pelleted and
730 resuspended in PBS. Upon 1 h incubation at 100°C, an equal volume of phenol was added, and
731 samples were incubated at 70°C for 1.5 h. Samples were centrifuged at 20000 xg at 4°C for 30
732 min, then the water phase was recovered. SDS-PAGE samples were prepared by adding 1:2 tris-
733 glycine loading buffer and incubated for 2 min at 85°C. SDS-PAGE gel was transferred onto PVDF
734 membrane using the iBlot™ Gel Transfer Device and Stacks (Thermo Fisher). Membranes were
735 blocked for 1h at room temperature in TBS 1x/0.1% Tween-20/5% milk. Purified mAbs were used
736 at 1µg/mL in TBS 1x/0.1% Tween-20/5% milk. Following an overnight incubation at 4°C,
737 membranes were washed 3 times with TBS 1x/0.1% Tween-20. Incubation with secondary
738 antibody (goat anti-human Fab) diluted 1:75000 in TBS 1x/0.1% Tween-20/5% milk was carried
739 out for 1 h at room temperature. Membranes were washed 3 times in TBS 1x/0.1% Tween-20
740 and then developed with chemiluminescence readout.

741

742 ## Characterization of mAb binding by high-resolution and high-content confocal microscopy

743 A single colony of bacteria was picked from an LB-agar plate and grown ON in LB with 5 µg/mL
744 meropenem. $ST147_{NDM1}$ stably expressing super-folder(sf)mCherry were grown in LB with 150
745 µg/mL hygromycin. The overnight culture was diluted in LB without antibiotics to OD_{600} 0.025 or
746 0.05 and plated into a 96-well Phenoplate (Perkin Elmer, 6055300). Upon incubation for 2 h at
747 37°C without CO_2 in static conditions, adherent bacteria were fixed in 4% paraformaldehyde
748 (PFA)/PBS (Thermo Fisher) or Cytofix (BD) for 15 min at RT. Alternatively, overnight grown
749 bacteria were re-launched in LB with antibiotics until exponential phase (OD_{600} 0.4-0.6). Then,
750 bacteria were pelleted, resuspended in PBS at OD_{600} 0.25 and transferred into a 96-well
751 Phenoplate. Finally, samples were briefly spinned at the bottom of the plate before fixation in
752 4% PFA.

753 For experiments aimed at staining a single anti-Kp mAb, selected antibodies were diluted in a
754 solution of PBS/1% BSA at a concentration of 0.5 µg/mL and incubated for 30 min at RT. Then,
755 samples were washed in PBS and a mixture of goat anti-Human Alexa488 conjugated secondary
756 antibody (Thermo Fisher, diluted 1:2000) and DAPI (Thermo Fisher, diluted 1:2000) in
757 PBS/BSA1% was added for 30 min at RT. Finally, samples were washed in PBS and 50 µL of 1%
758 Low Melting (LM) agarose (Sigma) were distributed in each well. Samples were stored at 4°C and
759 imaging was performed within the following 24 hours.

760 For experiments in which multiple anti-Kp mAbs were simultaneously stained, antibodies were
761 previously conjugated with Alexa488, Alexa555 and Alexa647 fluorophores, using the Zip Alexa
762 Fluor™ Rapid Antibody Labelling Kits (Thermo Fisher) following manufacturer instructions. After
763 fixation, samples were first blocked in PBS/1% BSA for 30 min at RT and then incubated with a
764 mixture of fluorophore-conjugated mAbs (each one at 1 µg/mL) and DAPI (1:2000) in PBS/1%
765 BSA. Following 30 min incubation at RT, samples were washed in PBS and prepared for imaging
766 by adding 50 µL of 1% LM agarose. Samples were imaged on the following day.

767

768 ## Construction of sfmCherry-expressing recombinant Kp strain

769 The $ST147_{NDM-1}$ strain expressing sfmCherry under control of the pTAC promoter was obtained
770 as follows. Codon-optimized tandem copies of the sfmCherry gene fused to the pTAC promoter
771 were synthesized by GeneArt (Thermo Fisher Scientific) and cloned into the HindIII and SpeI
772 restriction sites of the pSEVA23a1 vector[79] where a hygromycin resistance cassette had been
773 inserted in BamHI and XbaI. Two copies of sfmCherry were employed to maximise expression of
774 the fluorescent protein, according to what had been reported by Kolbe and colleagues[80].
775 Restriction enzymes were from New England Biolabs. $ST147_{NDM-1}$ was transformed by
776 electroporation with the resulting plasmid using an Eporator instrument (Eppendorf) and
777 transformants were selected on LB agar plates containing 150 μg/mL hygromycin. Transformants
778 were validated by colony PCR and expression of sfmCherry was verified by flow cytometry and
779 confocal microscopy. One of the transformed colonies was saved for further analyses.
780

781 ## Complementation of $ST147_{NDM-9}$ strain

782 The O-antigen-negative phenotype of the $ST147_{NDM-9}$ Kp strain was complemented as follows.
783 The *wbbO* gene of $ST147_{NDM-1}$ Kp, retrieved by whole genome sequencing, was synthesized by
784 GeneArt (Thermo Fisher Scientific) and cloned, under control of the pTAC promoter, into the
785 HindIII and SpeI restriction sites of the pSEVA23a1 vector[79] where a hygromycin resistance
786 cassette had been inserted in BamHI and XbaI (all restriction enzymes were from New England
787 Biolabs). Correct cloning was confirmed by Sanger sequencing (Eurofins). $ST147_{NDM-9}$ was
788 transformed by electroporation with the resulting construct according to standard procedures
789 using an Eporator instrument (Eppendorf). Transformants were selected on LB agar plates
790 containing 150 μg/mL hygromycin. One of the selected colonies was named $ST147_{NDM-}$
791 $_{9}$/pSEVA23a1_*wbbO* and saved for further analyses.
792

793 ## Opsonophagocytosis assay

794 THP-1 cells (ATCC) were maintained in RPMI 1640 containing GlutaMax (Thermo Fisher) and
795 complemented with 10 mM Hepes (Thermo Fisher), 1 mM Sodium Pyruvate (Thermo Fisher) and
796 10% fetal bovine serum (FBS) (Thermo Fisher). Three days before the assay, 50,000 cells per well

797 were seeded into a 96-well black-shielded Optiplate (Perkin Elmer) in the presence of 20 ng/mL
798 phorbol-12-myristate-13-acetate (PMA) to promote monocyte differentiation into macrophages.
799 The day after, PMA was washed out and cells were maintained in fresh medium for two
800 additional days.
801 Infection of macrophage was performed using $ST147_{NDM1}$-sfmCherry expressing Kp. Bacteria
802 were grown ON and re-launched the following morning to reach OD_{600} 0.5. After centrifugation,
803 bacteria were resuspended in phagocytosis media (RPMI 1640+GlutaMax, 10 mM Hepes, 1 mM
804 Sodium Pyruvate) to have a 1:2 dilution of the initial culture volume. To allow bacterial
805 opsonization, mAbs dilutions were prepared in 25 μL of phagocytosis media and incubated with
806 25 μL of bacteria for 30 min at 37°C in shaking conditions (500 rpm). This mixture was then added
807 to differentiated macrophages and centrifuged for 3 min at room temperature to synchronize
808 the infection. Following the incubation of 1 hour at 37°C in the presence of 5% CO_2, samples were
809 treated for an additional hour with 150 μg/mL streptomycin to kill not engulfed bacteria. Finally,
810 samples were incubated for 5 min at room temperature with PBS/0.1% Triton-X100 to
811 permeabilize cells and allow the release of internalised bacteria in the supernatants. Bacterial
812 fluorescence was read using a Varioskan Lux microplate reader (Thermo Fisher) as a readout of
813 the uptaken bacteria.
814

815 ### Live bacterial imaging

816 $ST147_{NDM-1}$-sfmCherry was grown ON as described before and re-launched until OD_{600} 0.5. The
817 assay was carried out in a final volume of 50 μL containing exponential Kp diluted 1:100, 12.5%
818 BRC and escalating doses of anti-Kp mAbs in PBS. Samples were prepared in 96-well Phenoplate
819 (Perkin Elmer, 6055300) and briefly centrifuged at 1000 rpm to keep bacteria closer to the
820 bottom of the well. Acquisition started immediately after centrifugation and was carried out at
821 37°C by acquiring frames every 2 min for 2 hours.
822

823 ### Microscopy and image analysis

824 Imaging was performed using the Opera Phenix platform (Perkin Elmer) and all samples were
825 acquired using a 63X N.A. 1.15 water objective.

826 For mAb binding experiments carried out in fixed conditions, 20 fields of view (FOV)/well were
827 selected. For each FOV, five z-stacks separated by a z-step of 0.5 µm were acquired. Imaging was
828 performed in confocal mode by exciting the samples with lasers at 425 nm, 488 nm and 561 nm
829 and collecting the emitted light using bandpass filters 435-480 nm, 500-550 nm and 570-630nm,
830 respectively.
831 For bacterial live imaging experiments, 3 FOV/well were acquired and three z-stacks separated
832 by a z-step of 0.5 µm were imaged. Imaging was performed in widefield mode by exciting the
833 samples with lasers at 561nm and collecting the light using the bandpass emission filter 570-630
834 nm.
835 Images were analyzed with Harmony (v4.9), provided by Perkin Elmer, by using custom-made
836 image analysis pipeline described in Table S5. Individual bacteria were detected using the DAPI
837 channel and filtered according to their morphology based on data available in literature. To
838 measure mAb intensity levels, the mean intensity of the A488 signal was measured within a ROI
839 drawn around each bacterium (**Figure S5**). To measure mAb occupancy area, A488 spots were
840 detected, and their morphology features were measured. A488 spots displaying an area smaller
841 than 0.5 μm^2 were discarded from the analysis because they were not representative of the
842 distribution of the mAb signals around the bacteria.
843

844 ## Purification of $ST147_{NDM-1}$ capsule and purification of O-antigen from Kp strains

845 Capsule and O-antigens were purified according to slightly modified procedures already published [81,83].
846

847 ## Nuclear magnetic resonance spectroscopy (NMR)

848 10 mg of purified capsule and O antigen material was buffer-exchanged to D_2O by drying with a
849 SpeedVac and resuspending in 99.9 % D_2O for 3 times in total. NMR spectra (1H, HSQC, 13C)
850 were recorded at 323 K on Bruker AVANCE NEO and AVANCE MHD NMR spectrometers,
851 operating at 900 and 950 MHz (1H Larmor frequency), respectively, both equipped with triple
852 resonance cryo-probes. The obtained spectra were compared with previously published ones to
853 confirm capsule[82] and O-antigen[48,84] identity.
854

855 ELISA on purified Kp O-antigen and capsule

856 To perform the ELISA, purified O2a-LPS and O2afg -LPS were kindly provided by Chris Whitfield's
857 group[48]. In addition, in-house purified KL64 capsule and O2a and O1 O-antigens were used to
858 coat high-binding 384-well plates (Greiner ref. 781061) and incubated at 4°C ON. The next day,
859 plates were blocked in PBS-BSA 1% at 37°C for 1h. After blocking, plates were incubated with
860 each mAb as primary antibody at a final concentration of 10 µg/ml for 2h at RT, in the presence
861 of PBS, 1% BSA, and 0.05% Tween-20. Next, anti-human IgG secondary antibody conjugated with
862 Alkaline Phosphatase (Southern Biotech) was added for 1h at 37°C. To detect antigen-mAbs
863 binding, pNPP (p-nitrophenyl phosphate; Sigma-Aldrich) was used as a soluble substrate, and the
864 final reaction was quantified at a wavelength of 405 nm using the Varioskan Lux Reader. After
865 each incubation step, plates were washed three times with 100 µl per well of washing buffer
866 (PBS plus 0.05% Tween-20). Sample buffer and an unrelated mAb were used respectively as blank
867 and negative control, and we considered positive hits those wells showing an OD_{405} value 3-fold
868 higher than the blank. As a positive control, a 1:100 dilution of pooled plasma from different
869 patients was used.

870 Immunocompetent $ST147_{NDM-1}$ bacteremia model

871 This portion of the study was done in the laboratory of Dr. David P. Nicolau and Dr. Kamilia
872 Abdelraouf, at the Center for Anti-infective Research and Development, Hartford Hospital.
873 Specific pathogen-free, female ICR mice weighing 20-22 grams were obtained from Charles River
874 Laboratories, Inc., (Wilmington, MA). The animals were allowed to acclimate for a minimum of
875 48 h before commencement of experimentation and were provided food and water *ad libitum*
876 [85,86]. The protocol was reviewed and approved by the Institutional Animal Care and Use
877 Committee at Hartford Hospital. Mice were administered uranyl nitrate 5 mg/kg three days prior
878 to inoculation to produce a controlled degree of renal impairment. $ST147_{NDM-1}$ was previously
879 frozen at - 80°C in skim milk (BD BioSciences, Sparks, MD). Prior to mice inoculation, two transfers
880 of the organisms were performed onto Trypticase Soy Agar plates with 5% sheep blood (TSA II™;
881 Becton, Dickinson & Co.; Sparks, MD) and incubated at 37°C for approximately 24 h. After 18-24
882 h of incubation of the second transfer, a bacterial suspension of approximating $10^{6.5}$ CFU/ml in
883 5% hog gastric mucin was made for inoculation. Final inoculum concentrations were confirmed

884 by serial dilution and plating techniques. Septicemia was produced by IP injection of 0.5 ml of
885 the inoculum.
886 08O09, 05N02 and 05D08 were reconstituted with PBS to the concentrations required to deliver
887 1, 5, 10, and 20 mg/kg doses based on the mean weight of the study mice population. All dosing
888 solutions were kept on ice while filled syringes with dosing solutions were refrigerated until use.
889 PBS solution with a pH of 7.4 was utilized as the vehicle for dosing control animals throughout
890 the study.
891 For PRO studies, single dose mAb 08O09, 05N02 or 05D08 of 1, 5, 10, 20 mg/kg were
892 administered through intraperitoneal (IP) route 24 h prior to bacterial inoculation (Figure 5A).
893 For THR studies, single dose 08O09 of 1, 5, 10, 20 mg/kg were administered through intravenous
894 (IV) route 1 h post bacterial inoculation (Figure 5F). For PRO+THR studies, one dose of 1 or 5
895 mg/kg of 08O09 was administered IP 24 h prior to bacterial inoculation, and a second dose of
896 08O09 at the same dose was administered IV 1 h post bacterial inoculation (Figure 5H). Each
897 dosing regimen consisted of 10 mice per group. Sham control mice (n=10) received PBS in the
898 same volume, route, and schedule as the study groups. One hour after inoculation, the 0 h
899 control group of 6 mice was euthanized by CO2 exposure followed by cervical dislocation for
900 spleen harvest. Spleens were homogenized and serial dilutions of the samples were plated on
901 agar for CFU determination to confirm the establishment of septicemia. Sham controls as well as
902 the study group mice were followed up for mortality for 96 h. Spleens were harvested and
903 processed as previously described for CFU determination, from the mice that are euthanized or
904 found dead during the observation time. Animals survived till 96 h were euthanized and spleens
905 were also harvested and processed for CFU enumeration.
906 Efficacy was calculated as the reduction in spleen bacterial load ($\log_{10}$ CFU) comparing mice
907 received therapy with sham control. The rate and extent of mortality were recorded and
908 assessed over the four-day (96 h) study period. Bacterial density reductions were analyzed using
909 one-way ANOVA with Tukey's analyses. Survivals were compared between groups using Kaplan-
910 Meier survival analysis and the log rank test.
911 Additionally, plasma concentration of 08O09 in uninfected mice were assessed for PRO and THR
912 5 mg/kg regimens. Mice were prepared as previously described. Plasma was collected through

913 orbital bleeding at baseline for all mice as control samples for analysis. One group of 6 mice were
914 then administered IP single dose of 08O09 5 mg/kg. At 24 h post-dose, plasma was collected
915 through cardiac puncture after euthanasia. Blood samples were collected in vials containing K2
916 EDTA. The blood was centrifuged and the plasma from each sample was transferred into
917 polypropylene tubes. These tubes were stored at -80 °C until plasma concentrations were
918 determined. The plasma concentrations of 08O09 were determined by quantitative ELISA, as
919 described in previous section. Each plasma concentration was evaluated in 5 replicates and the
920 values from the replicates were averaged for each sample. Values were obtained after 20 min
921 measurement of the plates and interpolated from a sigmoidal curve of 08O09 in presence of
922 mice plasma.
923
924
925
926

927 ## SUPPLEMENTAL VIDEOS

928

929 **SupplementalVideo1_Cluster1 mAb.** Time-lapse imaging of $ST147_{NDM-1}$-sfmCherry treated with
930 100 µg/mL of anti-Kp mAb 08O09.

931 **SupplementalVideo2_Cluster2 mAb.** Time- lapse imaging of $ST147_{NDM-1}$-sfmCherry treated with
932 100 µg/mL of anti-Kp mAb 05N02.

933

934

935 REFERENCES

936 1. World Health Organization. (2021). 10 Global health issues to track in 2021.
937 https://www.who.int/news-room/spotlight/10-global-health-issues-to-track-in-
938 2021.

939 2. World Health Organization. (2024). WHO priority pathogens list for R&D of new
940 antibiotics. https://www.who.int/news/item/27-02-2017-who-publishes-list-of-
941 bacteria-for-which-new-antibiotics-are-urgently-needed.

942 3. Arcari, G., and Carattoli, A. (2023). Global spread and evolutionary convergence of
943 multidrug-resistant and hypervirulent *Klebsiella pneumoniae* high-risk clones.
944 Pathog Glob Health *117*, 328–341. 10.1080/20477724.2022.2121362.

945 4. Wantuch, P.L., and Rosen, D.A. (2023). Klebsiella pneumoniae: adaptive immune
946 landscapes and vaccine horizons. Preprint at Elsevier Ltd, 10.1016/j.it.2023.08.005
947 10.1016/j.it.2023.08.005.

948 5. Gonzalez-Ferrer, S., Peñaloza, H.F., Budnick, J.A., Bain, W.G., Nordstrom, H.R., Lee,
949 J.S., and Van Tyne, D. (2021). Finding order in the chaos: Outstanding questions in
950 Klebsiella pneumoniae Pathogenesis. Infect Immun *89*. 10.1128/IAI.00693-20.

951 6. Falcone, M., Daikos, G.L., Tiseo, G., Bassoulis, D., Giordano, C., Galfo, V., Leonildi,
952 A., Tagliaferri, E., Barnini, S., Sani, S., et al. (2021). Efficacy of Ceftazidime-
953 avibactam Plus Aztreonam in Patients With Bloodstream Infections Caused by
954 Metallo-β-lactamase–Producing Enterobacterales. Clinical Infectious Diseases *72*,
955 1871–1878. 10.1093/cid/ciaa586.

956 7. Baker, S., Thomson, N., Weill, F.-X., and Holt, K.E. (2018). Genomic insights into the
957 emergence and spread of antimicrobial-resistant bacterial pathogens. Science
958 (1979) *360*, 733–738. 10.1126/science.aar3777.

959 8. Podschun, R., and Ullmann, U. (1998). *Klebsiella* spp. as Nosocomial Pathogens:
960 Epidemiology, Taxonomy, Typing Methods, and Pathogenicity Factors. Clin
961 Microbiol Rev *11*, 589–603. 10.1128/CMR.11.4.589.

962 9. Shon, A.S., Bajwa, R.P.S., and Russo, T.A. (2013). Hypervirulent
963 (hypermucoviscous) *Klebsiella pneumoniae*. Virulence *4*, 107–118.
964 10.4161/viru.22718.

965 10. Lam, M.M.C., Wick, R.R., Watts, S.C., Cerdeira, L.T., Wyres, K.L., and Holt, K.E.
966 (2021). A genomic surveillance framework and genotyping tool for Klebsiella
967 pneumoniae and its related species complex. Nat Commun *12*, 4188.
968 10.1038/s41467-021-24448-3.

969 11. Lan, P., Jiang, Y., Zhou, J., and Yu, Y. (2021). A global perspective on the
970 convergence of hypervirulence and carbapenem resistance in Klebsiella
971 pneumoniae. Preprint at Elsevier Ltd, 10.1016/j.jgar.2021.02.020
972 10.1016/j.jgar.2021.02.020.

973 12. Samuelsen, Ø., Toleman, M.A., Hasseltvedt, V., Fuursted, K., Leegaard, T.M.,
974 Walsh, T.R., Sundsfjord, A., and Giske, C.G. (2011). Molecular characterization of
975 VIM-producing Klebsiella pneumoniae from Scandinavia reveals genetic
976 relatedness with international clonal complexes encoding transferable multidrug
977 resistance. Clinical Microbiology and Infection *17*, 1811–1816. 10.1111/j.1469-
978 0691.2011.03532.x.

979 13. Hamzaoui, Z., Ocampo-Sosa, A., Maamar, E., Fernandez Martinez, M., Ferjani, S.,
980 Hammami, S., Harbaoui, S., Genel, N., Arlet, G., Saidani, M., et al. (2018). An
981 Outbreak of NDM-1-Producing *Klebsiella pneumoniae* , Associated with OmpK35
982 and OmpK36 Porin Loss in Tunisia. Microbial Drug Resistance *24*, 1137–1147.
983 10.1089/mdr.2017.0165.

984 14. Peirano, G., Chen, L., Kreiswirth, B.N., and Pitout, J.D.D. (2020). Emerging
985 Antimicrobial-Resistant High-Risk Klebsiella pneumoniae Clones ST307 and ST147.
986 Antimicrob Agents Chemother *64*. 10.1128/AAC.01148-20.

987 15. Li, J., Nation, R.L., Milne, R.W., Turnidge, J.D., and Coulthard, K. (2005). Evaluation
988 of colistin as an agent against multi-resistant Gram-negative bacteria. Int J
989 Antimicrob Agents *25*, 11–25. 10.1016/j.ijantimicag.2004.10.001.

990 16. Wolinsky, E., and Hines, J.D. (1962). Neurotoxic and Nephrotoxic Effects of Colistin
991 in Patients with Renal Disease. New England Journal of Medicine *266*, 759–762.
992 10.1056/NEJM196204122661505.

993 17. Lim, L.M., Ly, N., Anderson, D., Yang, J.C., Macander, L., Jarkowski, A., Forrest, A.,
994 Bulitta, J.B., and Tsuji, B.T. (2010). Resurgence of Colistin: A Review of Resistance,
995 Toxicity, Pharmacodynamics, and Dosing. Pharmacotherapy: The Journal of Human
996 Pharmacology and Drug Therapy *30*, 1279–1291. 10.1592/phco.30.12.1279.

997 18. Pathogen Watch. (2024). Global distribution of ST147 in PathogenWatch.
998 https://pathogen.watch/genomes/all/map?genusId=570&mlst=147&speciesId=57
999 3.

1000 19. Di Pilato, V., Henrici De Angelis, L., Aiezza, N., Baccani, I., Niccolai, C., Parisio, E.M.,
1001 Giordano, C., Camarlinghi, G., Barnini, S., Forni, S., et al. (2022). Resistome and
1002 virulome accretion in an NDM-1-producing ST147 sublineage of Klebsiella
1003 pneumoniae associated with an outbreak in Tuscany, Italy: a genotypic and
1004 phenotypic characterisation. Lancet Microbe *3*, e224–e234. 10.1016/S2666-
1005 5247(21)00268-8.

1006 20. Martin, M.J., Corey, B.W., Sannio, F., Hall, L.R., Macdonald, U., Jones, B.T., Mills,
1007 E.G., Harless, C., Stam, J., Maybank, R., et al. (2021). Anatomy of an extensively
1008 drug-resistant Klebsiella pneumoniae outbreak in Tuscany, Italy. PNAS *118*, 1–8.
1009 10.1073/pnas.2110227118/-/DCSupplemental.

1010 21. Tavoschi, L., Forni, S., Porretta, A., Righi, L., Pieralli, F., Menichetti, F., Falcone, M.,
1011 Gemignani, G., Sani, S., Vivani, P., et al. (2020). Prolonged outbreak of New Delhi

1012 metallo-betalactamase-producing carbapenem-resistant Enterobacterales (NDM-
1013 CRE), Tuscany, Italy, 2018 to 2019. Preprint, 10.2807/1560-
1014 7917.ES.2020.25.6.2000085 10.2807/1560-7917.ES.2020.25.6.2000085.

1015 22. Starkova, P., Lazareva, I., Avdeeva, A., Sulian, O., Likholetova, D., Ageevets, V.,
1016 Lebedeva, M., Gostev, V., Sopova, J., and Sidorenko, S. (2021). Emergence of
1017 hybrid resistance and virulence plasmids harboring new delhi metallo-β-lactamase
1018 in klebsiella pneumoniae in russia. Antibiotics *10*. 10.3390/antibiotics10060691.

1019 23. Turton, J., Davies, F., Turton, J., Perry, C., Payne, Z., and Pike, R. (2019). Hybrid
1020 resistance and virulence plasmids in "high-risk" clones of klebsiella pneumoniae,
1021 including those carrying blandm-5. Microorganisms *7*.
1022 10.3390/microorganisms7090326.

1023 24. Ahmed, M.A.E.-G.E.-S., Yang, Y., Yang, Y., Yan, B., Chen, G., Hassan, R.M., Zhong, L.-
1024 L., Chen, Y., Roberts, A.P., Wu, Y., et al. (2021). Emergence of Hypervirulent
1025 Carbapenem-Resistant Klebsiella pneumoniae Coharboring a bla NDM-1 -Carrying
1026 Virulent Plasmid and a bla KPC-2 -Carrying Plasmid in an Egyptian Hospital .
1027 mSphere *6*. 10.1128/msphere.00088-21.

1028 25. Heiden, S.E., Hübner, N.O., Bohnert, J.A., Heidecke, C.D., Kramer, A., Balau, V.,
1029 Gierer, W., Schaefer, S., Eckmanns, T., Gatermann, S., et al. (2020). A Klebsiella
1030 pneumoniae ST307 outbreak clone from Germany demonstrates features of
1031 extensive drug resistance, hypermucoviscosity, and enhanced iron acquisition.
1032 Genome Med *12*. 10.1186/s13073-020-00814-6.

1033 26. Martin, M.J., Stribling, W., Ong, A.C., Maybank, R., Kwak, Y.I., Rosado-Mendez, J.A.,
1034 Preston, L.N., Lane, K.F., Julius, M., Jones, A.R., et al. (2023). A panel of diverse
1035 Klebsiella pneumoniae clinical isolates for research and development. Microb
1036 Genom *9*. 10.1099/mgen.0.000967.

1037 27. Rodrigues, C., Desai, S., Passet, V., Gajjar, D., and Brisse, S. (2022). Genomic
1038 evolution of the globally disseminated multidrug-resistant Klebsiella pneumoniae
1039 clonal group 147. Microb Genom *8*. 10.1099/mgen.0.000737.

1040 28. Troisi, M., Marini, E., Abbiento, V., Stazzoni, S., Andreano, E., and Rappuoli, R.
1041 (2022). A new dawn for monoclonal antibodies against antimicrobial resistant
1042 bacteria. Front Microbiol *13*. 10.3389/fmicb.2022.1080059.

1043 29. Banerjee, K., Motley, M.P., Boniche-Alfaro, C., Bhattacharya, S., Shah, R.,
1044 Ardizzone, A., and Fries, B.C. (2022). Patient-Derived Antibody Data Yields
1045 Development of Broadly Cross-Protective Monoclonal Antibody against ST258
1046 Carbapenem-Resistant Klebsiella pneumoniae . Microbiol Spectr *10*.
1047 10.1128/spectrum.01760-22.

1048 30. Diago-Navarro, E., Motley, M.P., Ruiz-Peréz, G., Yu, W., Austin, J., Seco, B.M.S.,
1049 Xiao, G., Chikhalya, A., Seeberger, P.H., Fries, B.C., et al. (2018). Novel, Broadly

1050 Reactive Anticapsular Antibodies against Carbapenem-Resistant Klebsiella
1051 pneumoniae Protect from Infection Downloaded from. 10.1128/mBio.

1052 31. Cohen, T.S., Pelletier, M., Cheng, L., Pennini, M.E., Bonnell, J., Cvitkovic, R., Chang,
1053 C.S., Xiao, X., Cameroni, E., Corti, D., et al. (2017). Anti-LPS antibodies protect
1054 against Klebsiella pneumoniae by empowering neutrophil-mediated clearance
1055 without neutralizing TLR4. JCI Insight *2*. 10.1172/jci.insight.92774.

1056 32. Pennini, M.E., De Marco, A., Pelletier, M., Bonnell, J., Cvitkovic, R., Beltramello, M.,
1057 Cameroni, E., Bianchi, S., Zatta, F., Zhao, W., et al. (2017). Immune stealth-driven
1058 O2 serotype prevalence and potential for therapeutic antibodies against multidrug
1059 resistant Klebsiella pneumoniae. Nat Commun *8*. 10.1038/s41467-017-02223-7.

1060 33. Rollenske, T., Szijarto, V., Lukasiewicz, J., Guachalla, L.M., Stojkovic, K., Hartl, K.,
1061 Stulik, L., Kocher, S., Lasitschka, F., Al-Saeedi, M., et al. (2018). Cross-specificity of
1062 protective human antibodies against Klebsiella pneumoniae LPS O-antigen. Nat
1063 Immunol *19*, 617–624. 10.1038/s41590-018-0106-2.

1064 34. Pennini, M.E., De Marco, A., Pelletier, M., Bonnell, J., Cvitkovic, R., Beltramello, M.,
1065 Cameroni, E., Bianchi, S., Zatta, F., Zhao, W., et al. (2017). Immune stealth-driven
1066 O2 serotype prevalence and potential for therapeutic antibodies against multidrug
1067 resistant Klebsiella pneumoniae. Nat Commun *8*, 1991. 10.1038/s41467-017-
1068 02223-7.

1069 35. Held, T.K., Jendrike, N.R.M., Rukavina, T., Podschun, R., and Trautmann, M. (2000).
1070 Binding to and Opsonophagocytic Activity of O-Antigen-Specific Monoclonal
1071 Antibodies against Encapsulated and Nonencapsulated *Klebsiella pneumoniae*
1072 Serotype O1 Strains. Infect Immun *68*, 2402–2409. 10.1128/IAI.68.5.2402-
1073 2409.2000.

1074 36. Wantuch, P.L., Knoot, C.J., Robinson, L.S., Vinogradov, E., Scott, N.E., Harding,
1075 C.M., and Rosen, D.A. (2023). Capsular polysaccharide inhibits vaccine-induced O-
1076 antigen antibody binding and function across both classical and hypervirulent
1077 K2:O1 strains of Klebsiella pneumoniae. PLoS Pathog *19*, e1011367.
1078 10.1371/journal.ppat.1011367.

1079 37. Follador, R., Heinz, E., Wyres, K.L., Ellington, M.J., Kowarik, M., Holt, K.E., and
1080 Thomson, N.R. (2016). The diversity of Klebsiella pneumoniae surface
1081 polysaccharides. Microb Genom *2*, e000073. 10.1099/mgen.0.000073.

1082 38. Kelly, S.D., Ovchinnikova, O.G., Müller, F., Steffen, M., Braun, M., Sweeney, R.P.,
1083 Kowarik, M., Follador, R., Lowary, T.L., Serventi, F., et al. (2023). Identification of a
1084 second glycoform of the clinically prevalent O1 antigen from Klebsiella
1085 pneumoniae. Proc Natl Acad Sci U S A *120*. 10.1073/pnas.2301302120.

1086 39. Kelly, S.D., Clarke, B.R., Ovchinnikova, O.G., Sweeney, R.P., Williamson, M.L.,
1087 Lowary, T.L., and Whitfield, C. (2019). Klebsiella pneumoniae O1 and O2ac
1088 antigens provide prototypes for an unusual strategy for polysaccharide antigen

1089 diversification. Journal of Biological Chemistry *294*, 10863–10876.
1090 10.1074/jbc.RA119.008969.

1091 40. Wang, Q., Chang, C.S., Pennini, M., Pelletier, M., Rajan, S., Zha, J., Chen, Y.,
1092 Cvitkovic, R., Sadowska, A., Thompson, J.H., et al. (2016). Target-agnostic
1093 identification of functional monoclonal antibodies against klebsiella pneumoniae
1094 multimeric mrka fimbrial subunit. Journal of Infectious Diseases *213*, 1800–1808.
1095 10.1093/infdis/jiw021.

1096 41. Hangartner, L., Zinkernagel, R.M., and Hengartner, H. (2006). Antiviral antibody
1097 responses: The two extremes of a wide spectrum. Preprint, 10.1038/nri1783
1098 10.1038/nri1783.

1099 42. Rossi, O., Molesti, E., Saul, A., Giannelli, C., Micoli, F., and Necchi, F. (2020). Intra-
1100 laboratory evaluation of luminescence based high-throughput serum bactericidal
1101 assay (L-sba) to determine bactericidal activity of human sera against shigella. High
1102 Throughput *9*. 10.3390/ht9020014.

1103 43. Aruta, M.G., Carducci, M., Micoli, F., Necchi, F., and Rossi, O. (2021). Increasing the
1104 High Throughput of a Luminescence-Based Serum Bactericidal Assay (L-SBA).
1105 BioTech *10*, 19. 10.3390/biotech10030019.

1106 44. Falcone, M., Giordano, C., Barnini, S., Tiseo, G., Leonildi, A., Malacarne, P.,
1107 Menichetti, F., and Carattoli, A. (2020). Extremely drug-resistant NDM-9-producing
1108 ST147 Klebsiella pneumoniae causing infections in Italy, May 2020.
1109 Eurosurveillance *25*. 10.2807/1560-7917.ES.2020.25.48.2001779.

1110 45. Wang, W., Tian, D., Hu, D., Chen, W., Zhou, Y., and Jiang, X. (2023). Different
1111 regulatory mechanisms of the capsule in hypervirulent Klebsiella pneumonia:
1112 “direct” wcaJ variation vs. “indirect” rmpA regulation. Front Cell Infect Microbiol
1113 *13*. 10.3389/fcimb.2023.1108818.

1114 46. Merrifield, E.H., and Stephen, A.M. (1979). STRUCTURAL STUDIES ON THE
1115 CAPSULAR POLYSACCHARIDE FROM Klebsiella SEROTYPE K64.

1116 47. Kos, V., and Whitfield, C. (2010). A membrane-located glycosyltransferase complex
1117 required for biosynthesis of the D-Galactan I lipopolysaccharide O antigen in
1118 Klebsiella pneumoniae. Journal of Biological Chemistry *285*, 19668–19678.
1119 10.1074/jbc.M110.122598.

1120 48. Clarke, B.R., Ovchinnikova, O.G., Kelly, S.D., Williamson, M.L., Butler, J.E., Liu, B.,
1121 Wang, L., Gou, X., Follador, R., Lowary, T.L., et al. (2018). Molecular basis for the
1122 structural diversity in serogroup O2-antigen polysaccharides in Klebsiella
1123 pneumoniae. Journal of Biological Chemistry *293*, 4666–4679.
1124 10.1074/jbc.RA117.000646.

1125 49. Apicella, M.A., Post, D.M.B., Fowler, A.C., Jones, B.D., Rasmussen, J.A., Hunt, J.R.,
1126 Imagaw, S., Choudhury, B., Inzana, T.J., Maier, T.M., et al. (2010). Identification,

1127 characterization and immunogenicity of an O-antigen capsular polysaccharide of
1128 Francisella tularensis. PLoS One *5*. 10.1371/journal.pone.0011060.

1129 50. de Jong, R.N., Beurskens, F.J., Verploegen, S., Strumane, K., van Kampen, M.D.,
1130 Voorhorst, M., Horstman, W., Engelberts, P.J., Oostindie, S.C., Wang, G., et al.
1131 (2016). A Novel Platform for the Potentiation of Therapeutic Antibodies Based on
1132 Antigen-Dependent Formation of IgG Hexamers at the Cell Surface. PLoS Biol *14*.
1133 10.1371/journal.pbio.1002344.

1134 51. Abdelraouf, K., Kim, A., Krause, K.M., and Nicolau, D.P. (2018). In vivo efficacy of
1135 plazomicin alone or in combination with meropenem or tigecycline against
1136 enterobacteriaceae isolates exhibiting various resistance mechanisms in an
1137 immunocompetent murine septicemia model. Antimicrob Agents Chemother *62*.
1138 10.1128/AAC.01074-18.

1139 52. Biedrzycka, M., Urbanowicz, P., Guzek, A., Brisse, S., Gniadkowski, M., and
1140 Izdebski, R. (2021). Dissemination of *Klebsiella pneumoniae* ST147 NDM-1 in
1141 Poland, 2015–19. Journal of Antimicrobial Chemotherapy *76*, 2538–2545.
1142 10.1093/jac/dkab207.

1143 53. Lapp, Z., Crawford, R., Miles-Jay, A., Pirani, A., Trick, W.E., Weinstein, R.A., Hayden,
1144 M.K., Snitkin, E.S., and Lin, M.Y. (2021). Regional Spread of *bla* NDM-1-Containing
1145 *Klebsiella pneumoniae* ST147 in Post-Acute Care Facilities. Clinical Infectious
1146 Diseases *73*, 1431–1439. 10.1093/cid/ciab457.

1147 54. Wyres, K.L., Nguyen, T.N.T., Lam, M.M.C., Judd, L.M., van Vinh Chau, N., Dance,
1148 D.A.B., Ip, M., Karkey, A., Ling, C.L., Miliya, T., et al. (2020). Genomic surveillance
1149 for hypervirulence and multi-drug resistance in invasive Klebsiella pneumoniae
1150 from South and Southeast Asia. Genome Med *12*, 11. 10.1186/s13073-019-0706-y.

1151 55. Wang, J., Shao, Y., Wang, W., Li, S., Xin, N., Xie, F., and Zhao, C. (2017). Caspase-11
1152 deficiency impairs neutrophil recruitment and bacterial clearance in the early
1153 stage of pulmonary Klebsiella pneumoniae infection. International Journal of
1154 Medical Microbiology *307*, 490–496. 10.1016/j.ijmm.2017.09.012.

1155 56. Xiong, H., Carter, R.A., Leiner, I.M., Tang, Y.-W., Chen, L., Kreiswirth, B.N., and
1156 Pamer, E.G. (2015). Distinct Contributions of Neutrophils and CCR2 $^{+}$ Monocytes to
1157 Pulmonary Clearance of Different Klebsiella pneumoniae Strains. Infect Immun *83*,
1158 3418–3427. 10.1128/IAI.00678-15.

1159 57. Ramirez-Moral, I., Blok, D.C., Bernink, J.H., Garcia-Laorden, M.I., Florquin, S., Boon,
1160 L., van't Veer, C., Mack, M., Saluzzo, S., Knapp, S., et al. (2021). Interleukin-33
1161 improves local immunity during Gram-negative pneumonia by a combined effect
1162 on neutrophils and inflammatory monocytes. J Pathol *253*, 374–383.
1163 10.1002/path.5601.

1164 58. Alvarez, D.A.´, Merino, S., Toma´s, J.M., Toma´s, T., Benedi´,Benedi´benedi´, V.J.,
1165 Sebastia´, S., Alberti´1, S., and Alberti´1, A. (2000). Capsular Polysaccharide Is a

1166 Major Complement Resistance Factor in Lipopolysaccharide O Side Chain-Deficient
1167 Klebsiella pneumoniae Clinical Isolates.

1168 59. Cortés, G., Borrell, N., de Astorza, B., Gómez, C., Sauleda, J., and Albertí, S. (2002).
1169 Molecular Analysis of the Contribution of the Capsular Polysaccharide and the
1170 Lipopolysaccharide O Side Chain to the Virulence of *Klebsiella pneumoniae* in a
1171 Murine Model of Pneumonia. Infect Immun *70*, 2583–2590.
1172 10.1128/IAI.70.5.2583-2590.2002.

1173 60. Regueiro, V., Campos, M.A., Pons, J., Albertí, S., and Bengoechea, J.A. (2006). The
1174 uptake of a Klebsiella pneumoniae capsule polysaccharide mutant triggers an
1175 inflammatory response by human airway epithelial cells. Microbiology (N Y) *152*,
1176 555–566. 10.1099/mic.0.28285-0.

1177 61. March, C., Cano, V., Moranta, D., Llobet, E., Pérez-Gutiérrez, C., Tomás, J.M.,
1178 Suárez, T., Garmendia, J., and Bengoechea, J.A. (2013). Role of Bacterial Surface
1179 Structures on the Interaction of Klebsiella pneumoniae with Phagocytes. PLoS One
1180 *8*, e56847. 10.1371/journal.pone.0056847.

1181 62. Camprubí, S. (1993). The role of the O-antigen lipopolysaccharide and capsule on
1182 an experimental Klebsiella pneumoniae infection of the rat urinary tract. FEMS
1183 Microbiol Lett *111*, 9–13. 10.1016/0378-1097(93)90175-2.

1184 63. Lawlor, M.S., Hsu, J., Rick, P.D., and Miller, V.L. (2005). Identification of *Klebsiella*
1185 *pneumoniae* virulence determinants using an intranasal infection model. Mol
1186 Microbiol *58*, 1054–1073. 10.1111/j.1365-2958.2005.04918.x.

1187 64. Held, T.K., Jendrike, N.R.M., Rukavina, T., Podschun, R., and Trautmann, M. (2000).
1188 Binding to and Opsonophagocytic Activity of O-Antigen-Specific Monoclonal
1189 Antibodies against Encapsulated and Nonencapsulated Klebsiella pneumoniae
1190 Serotype O1 Strains.

1191 65. Bansept, F., Schumann-Moor, K., Diard, M., Hardt, W.-D., Slack, E., and Loverdo, C.
1192 (2019). Enchained growth and cluster dislocation: A possible mechanism for
1193 microbiota homeostasis. PLoS Comput Biol *15*, e1006986.
1194 10.1371/journal.pcbi.1006986.

1195 66. Moor, K., Diard, M., Sellin, M.E., Felmy, B., Wotzka, S.Y., Toska, A., Bakkeren, E.,
1196 Arnoldini, M., Bansept, F., Co, A.D., et al. (2017). High-avidity IgA protects the
1197 intestine by enchaining growing bacteria. Nature *544*, 498–502.
1198 10.1038/nature22058.

1199 67. Zhou, K., Xiao, T., David, S., Wang, Q., Zhou, Y., Guo, L., Aanensen, D., Holt, K.E.,
1200 Thomson, N.R., Grundmann, H., et al. (2020). Novel Subclone of Carbapenem-
1201 Resistant *Klebsiella pneumoniae* Sequence Type 11 with Enhanced Virulence and
1202 Transmissibility, China. Emerg Infect Dis *26*, 289–297. 10.3201/eid2602.190594.

1203 68. Zhao, D., Shi, Q., Hu, D., Fang, L., Mao, Y., Lan, P., Han, X., Zhang, P., Hu, H., Wang,
1204 Y., et al. (2021). The Emergence of Novel Sequence Type Strains Reveals an

1205 Evolutionary Process of Intraspecies Clone Shifting in ICU-Spreading Carbapenem-
1206 Resistant Klebsiella pneumoniae. Front Microbiol *12*. 10.3389/fmicb.2021.691406.

1207 69. Struve, C., Roe, C.C., Stegger, M., Stahlhut, S.G., Hansen, D.S., Engelthaler, D.M.,
1208 Andersen, P.S., Driebe, E.M., Keim, P., and Krogfelt, K.A. (2015). Mapping the
1209 Evolution of Hypervirulent Klebsiella pneumoniae. mBio *6*. 10.1128/mBio.00630-
1210 15.

1211 70. Wang, J., Feng, Y., and Zong, Z. (2023). Worldwide transmission of ST11-KL64
1212 carbapenem-resistant *Klebsiella pneumoniae* : an analysis of publicly available
1213 genomes. mSphere *8*. 10.1128/msphere.00173-23.

1214 71. Andreano, E., Nicastri, E., Paciello, I., Pileri, P., Manganaro, N., Piccini, G., Manenti,
1215 A., Pantano, E., Kabanova, A., Troisi, M., et al. (2021). Extremely potent human
1216 monoclonal antibodies from COVID-19 convalescent patients. Cell *184*, 1821-
1217 1835.e16. 10.1016/j.cell.2021.02.035.

1218 72. Ye, J., Ma, N., Madden, T.L., and Ostell, J.M. (2013). IgBLAST: an immunoglobulin
1219 variable domain sequence analysis tool. Nucleic Acids Res *41*, W34–W40.
1220 10.1093/nar/gkt382.

1221 73. Chen, S., Zhou, Y., Chen, Y., and Gu, J. (2018). fastp: an ultra-fast all-in-one FASTQ
1222 preprocessor. Bioinformatics *34*, i884–i890. 10.1093/bioinformatics/bty560.

1223 74. Wick, R.R., Judd, L.M., Gorrie, C.L., and Holt, K.E. (2017). Unicycler: Resolving
1224 bacterial genome assemblies from short and long sequencing reads. PLoS Comput
1225 Biol *13*, e1005595. 10.1371/journal.pcbi.1005595.

1226 75. Lam, M.M.C., Wick, R.R., Judd, L.M., Holt, K.E., and Wyres, K.L. (2022). Kaptive 2.0:
1227 updated capsule and lipopolysaccharide locus typing for the Klebsiella
1228 pneumoniae species complex. Microb Genom *8*. 10.1099/mgen.0.000800.

1229 76. Page, A.J., Cummins, C.A., Hunt, M., Wong, V.K., Reuter, S., Holden, M.T.G.,
1230 Fookes, M., Falush, D., Keane, J.A., and Parkhill, J. (2015). Roary: rapid large-scale
1231 prokaryote pan genome analysis. Bioinformatics *31*, 3691–3693.
1232 10.1093/bioinformatics/btv421.

1233 77. Page, A.J., Taylor, B., Delaney, A.J., Soares, J., Seemann, T., Keane, J.A., and Harris,
1234 S.R. (2016). SNP-sites: rapid efficient extraction of SNPs from multi-FASTA
1235 alignments. Microb Genom *2*. 10.1099/mgen.0.000056.

1236 78. Nguyen, L.-T., Schmidt, H.A., von Haeseler, A., and Minh, B.Q. (2015). IQ-TREE: A
1237 Fast and Effective Stochastic Algorithm for Estimating Maximum-Likelihood
1238 Phylogenies. Mol Biol Evol *32*, 268–274. 10.1093/molbev/msu300.

1239 79. García-Gutiérrez, C., Aparicio, T., Torres-Sánchez, L., Martínez-García, E., de
1240 Lorenzo, V., Villar, C.J., and Lombó, F. (2020). Multifunctional SEVA shuttle vectors
1241 for actinomycetes and Gram-negative bacteria. Microbiologyopen *9*, 1135–1149.
1242 10.1002/mbo3.1024.

1243 80. Kolbe, K., Bell, A.C., Prosser, G.A., Assmann, M., Yang, H.-J., Forbes, H.E., Gallucci,
1244 S., Mayer-Barber, K.D., Boshoff, H.I., and Barry III, C.E. (2020). Development and
1245 Optimization of Chromosomally-Integrated Fluorescent Mycobacterium
1246 tuberculosis Reporter Constructs. Front Microbiol *11*. 10.3389/fmicb.2020.591866.

1247 81. Micoli, F., Giannelli, C., and Di Benedetto, R. (2021). O-antigen extraction,
1248 purification, and chemical conjugation to a carrier protein. In Methods in
1249 Molecular Biology 10.1007/978-1-0716-0795-4_14.

1250 82. Ravenscroft, N., Stephen, A.M., and Merrifield, E.H. (1987). Bacteriophage-
1251 associated lyase activity against Klebsiella serotype K64 capsular polysaccharide.
1252 Carbohydr Res *167*, 257–267. 10.1016/0008-6215(87)80283-5.

1253 83. Gormus, B.J., and Wheat, R.W. (1971). Polysaccharides of Type 6 Klebsiella. J
1254 Bacteriol *108*, 1304–1309. 10.1128/jb.108.3.1304-1309.1971.

1255 84. Vinogradov, E., Frirdich, E., MacLean, L.L., Perry, M.B., Petersen, B.O., Duus, J.Ø.,
1256 and Whitfield, C. (2002). Structures of Lipopolysaccharides from Klebsiella
1257 pneumoniae. Journal of Biological Chemistry *277*, 25070–25081.
1258 10.1074/jbc.M202683200.

1259 85. Landi, M.S., Kreider, J.W., Lang, C.M., and Bullock, L.P. (1982). Effects of shipping
1260 on the immune function in mice. Am J Vet Res *43*, 1654–1657.

1261 86. Obernier, J.A., and Baldwin, R.L. (2006). Establishing an Appropriate Period of
1262 Acclimatization Following Transportation of Laboratory Animals. ILAR J *47*, 364–
1263 369. 10.1093/ilar.47.4.364.

1264

1265

1266

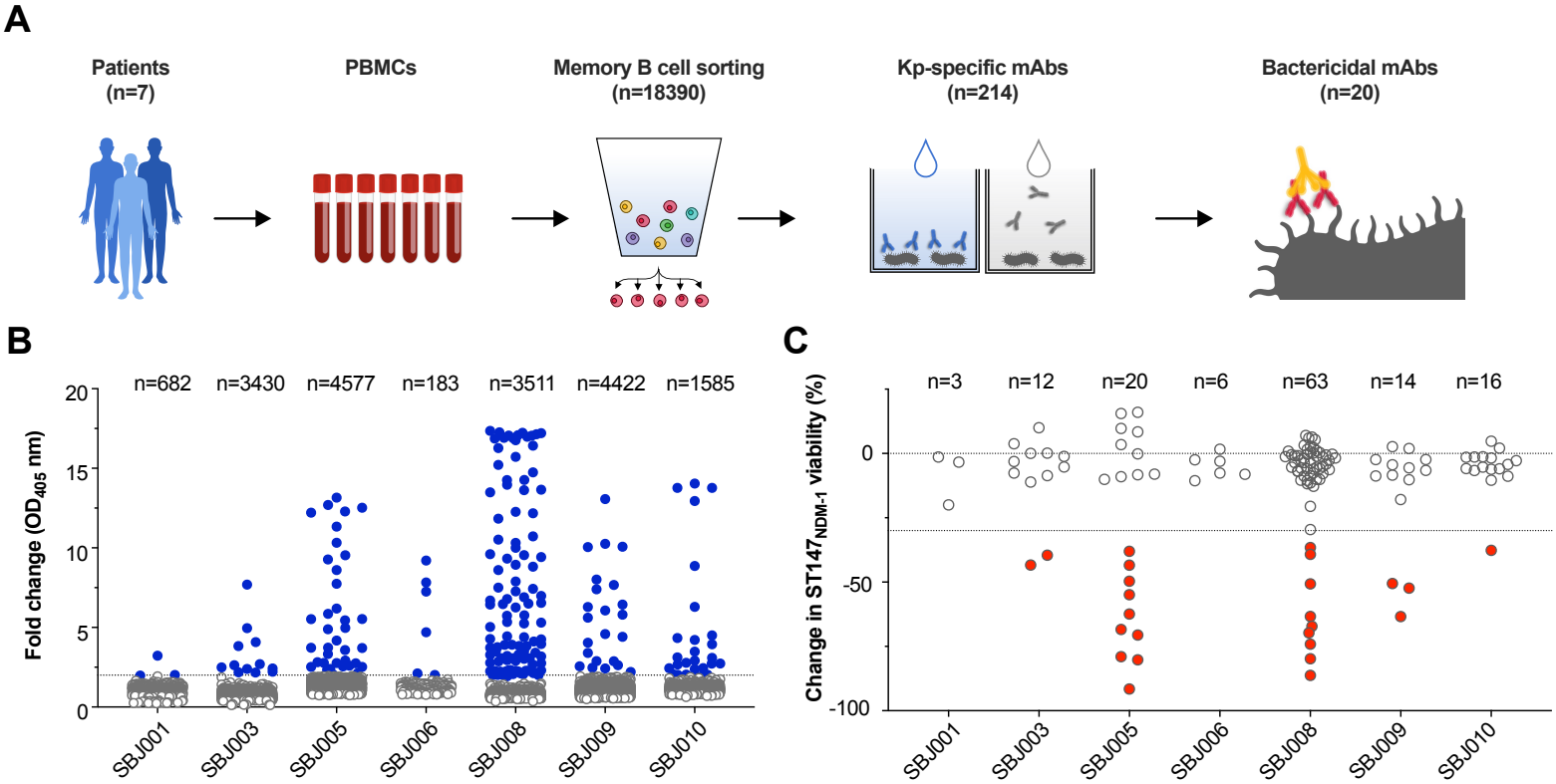
A
Patients
(n=7)
PBMCs
Memory B cell sorting
(n=18390)
Kp-specific mAbs
(n=214)
Bactericidal mAbs
(n=20)
B
n=682
n=3430
n=4577
n=183
n=3511
n=4422
n=1585
Fold change (OD405 nm)
20
15
10
5
0
SBJ001
SBJ003
SBJ005
SBJ006
SBJ008
SBJ009
SBJ010
C
n=3
n=12
n=20
n=6
n=63
n=14
n=16
Change in ST147NDM-1 viability (%)
0
-50
-100
SBJ001
SBJ003
SBJ005
SBJ006
SBJ008
SBJ009
SBJ010

Figure 1

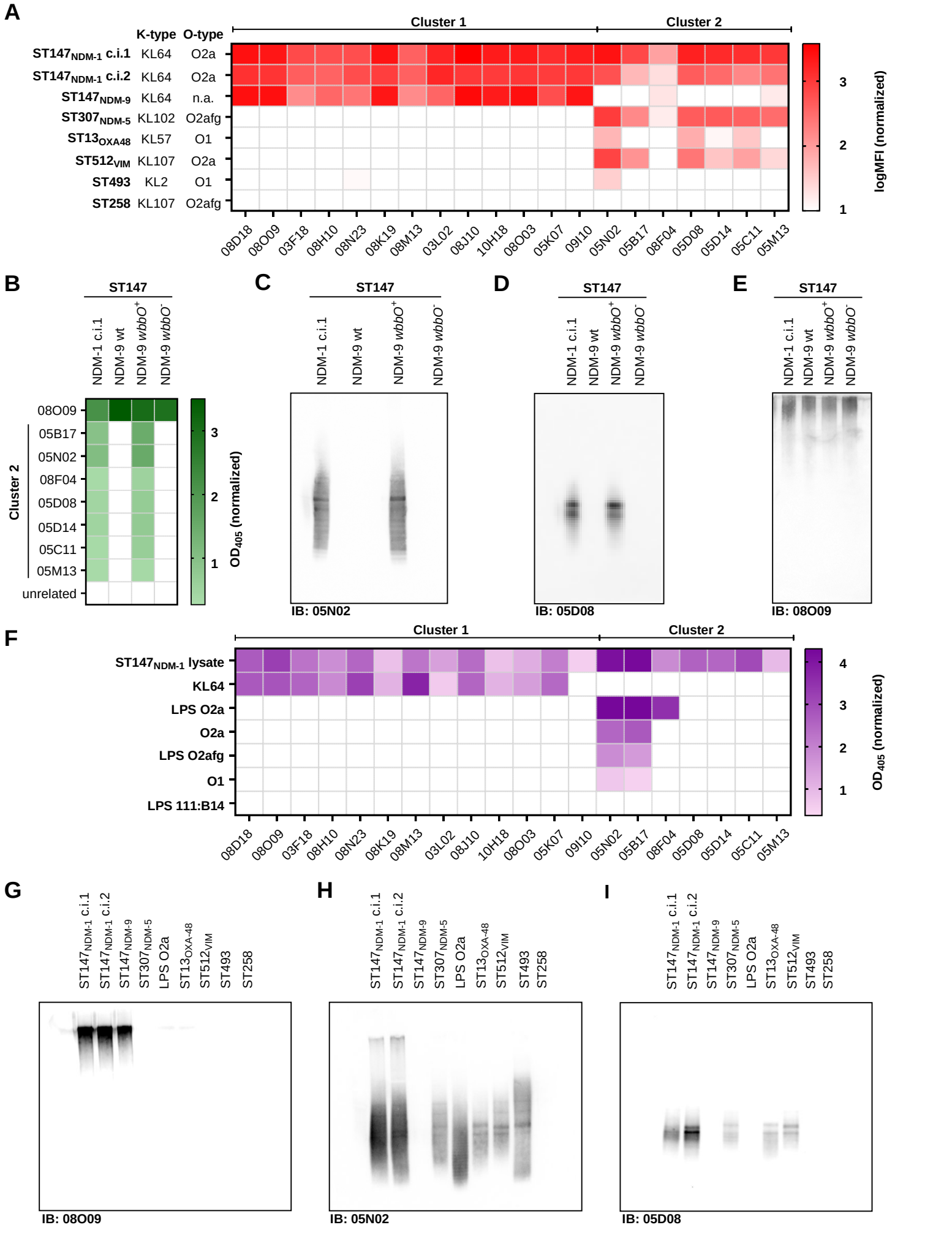
A
Cluster 1
Cluster 2
K-type
O-type
ST147NDM-1 c.i.1 KL64 O2a
ST147NDM-1 c.i.2 KL64 O2a
ST147NDM-9 KL64 n.a.
ST307NDM-5 KL102 O2afg
ST13OXA48 KL57 O1
ST512VIM KL107 O2a
ST493 KL2 O1
ST258 KL107 O2afg
08D18 08O09 03F18 08H10 08N23 08K19 08M13 03L02 08J10 10H18 08O03 05K07 09I10 05N02 05B17 08F04 05D08 05D14 05C11 05M13
logMFI (normalized)
B
ST147
NDM-1 c.i.1
NDM-9 wt
NDM-9 wbbO+
NDM-9 wbbO-
Cluster 2
08O09
05B17
05N02
08F04
05D08
05D14
05C11
05M13
unrelated
OD405 (normalized)
C
IB: 05N02
D
IB: 05D08
E
IB: 08O09
F
ST147NDM-1 lysate
KL64
LPS O2a
O2a
LPS O2afg
O1
LPS 111:B14
OD405 (normalized)
G
ST147NDM-1 c.i.1
ST147NDM-1 c.i.2
ST147NDM-9
ST307NDM-5
LPS O2a
ST13OXA-48
ST512VIM
ST493
ST258
IB: 08O09
H
IB: 05N02
I
IB: 05D08

Figure 2

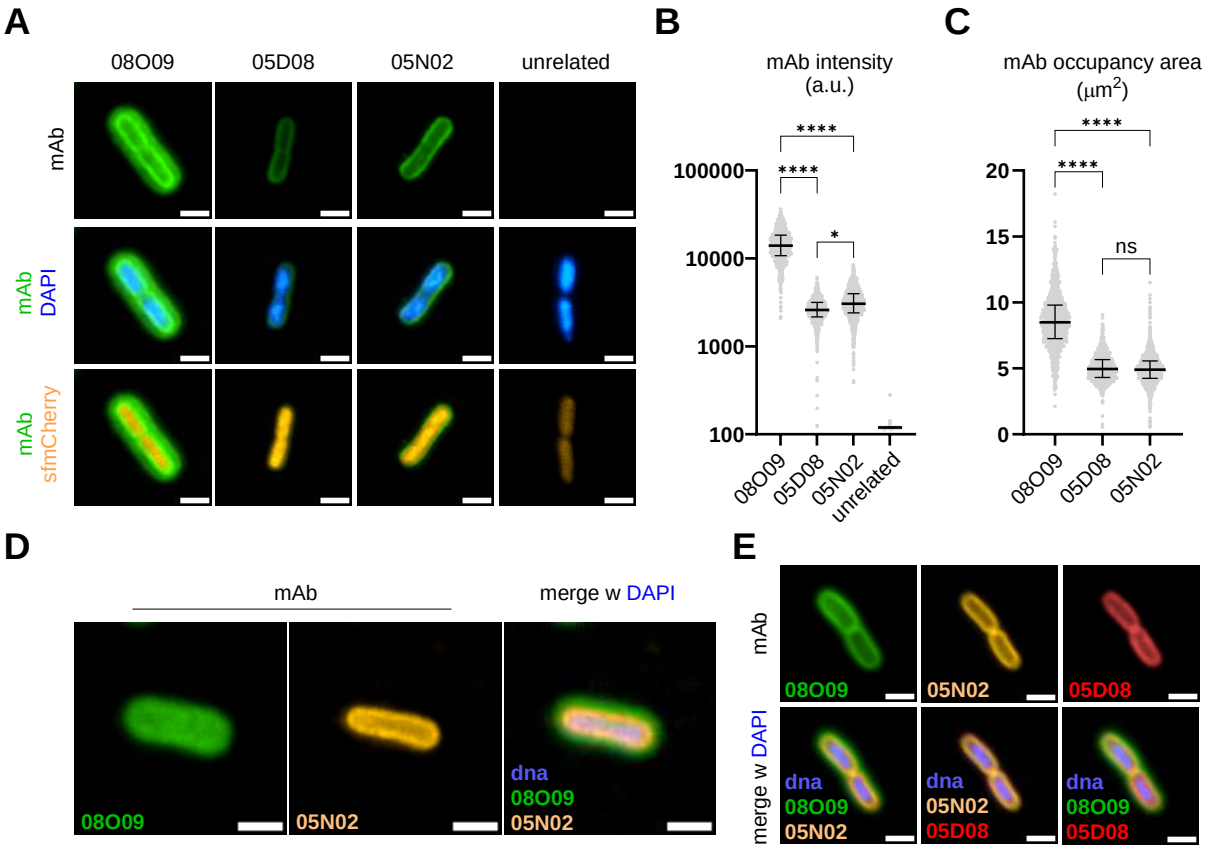
A
08O09
05D08
05N02
unrelated
mAb
mAb
DAPI
mAb
sfmCherry
B
mAb intensity
(a.u.)
****
****
*
100000
10000
1000
100
08O09
05D08
05N02
unrelated
C
mAb occupancy area
(μm2)
****
****
ns
20
15
10
5
0
08O09
05D08
05N02
D
mAb
merge w DAPI
08O09
05N02
dna
08O09
05N02
E
mAb
merge w DAPI
08O09
05N02
05D08
dna
08O09
05N02
dna
05N02
05D08
dna
08O09
05D08

Figure 3

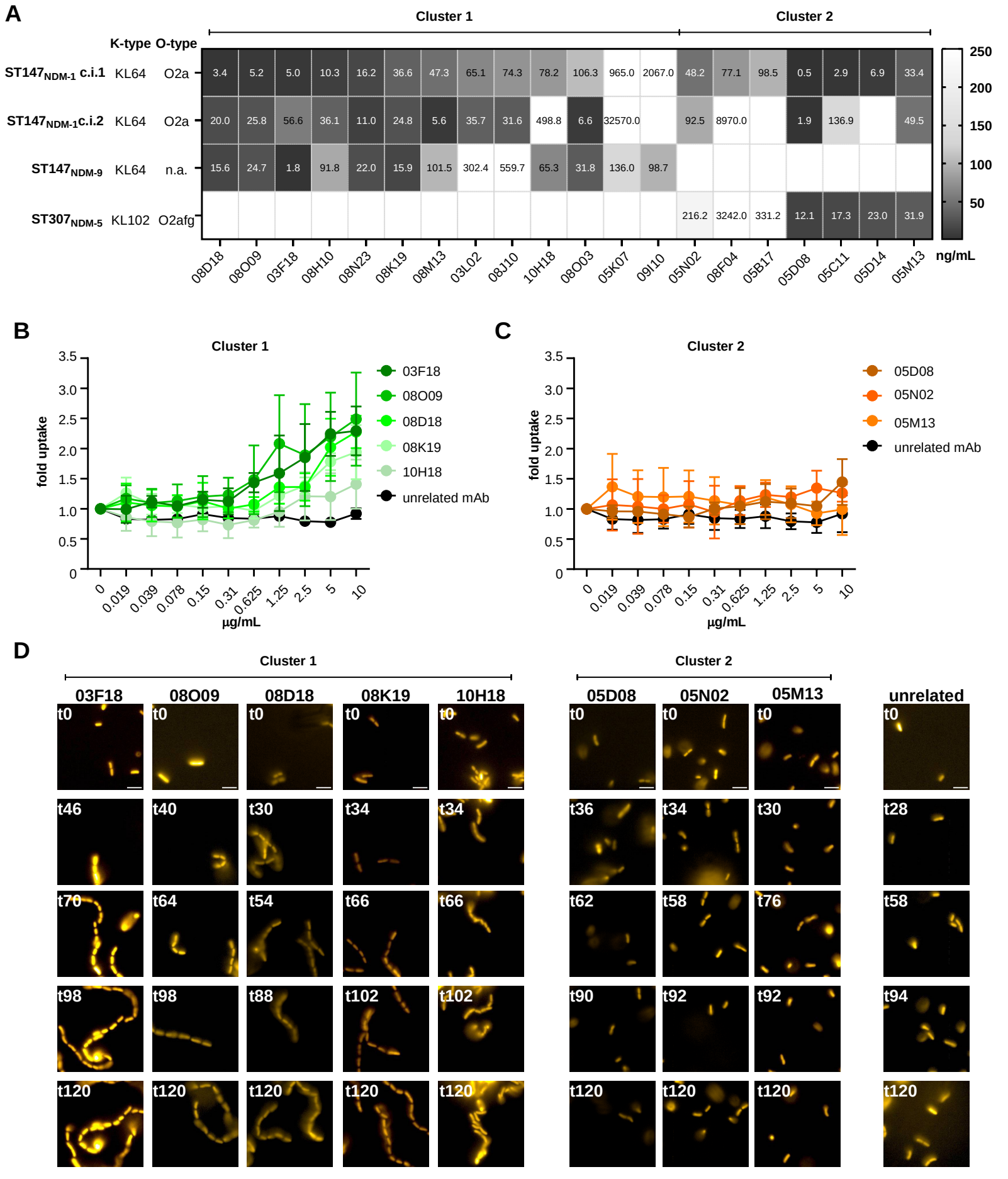
A
Cluster 1
Cluster 2
K-type O-type
ST147NDM-1 c.i.1 KL64 O2a
ST147NDM-1c.i.2 KL64 O2a
ST147NDM-9 KL64 n.a.
ST307NDM-5 KL102 O2afg
08D18 08O09 03F18 08H10 08N23 08K19 08M13 03L02 08J10 10H18 08O03 05K07 09I10 05N02 08F04 05B17 05D08 05C11 05D14 05M13
ng/mL
250 200 150 100 50
B
Cluster 1
fold uptake
03F18
08O09
08D18
08K19
10H18
unrelated mAb
µg/mL
C
Cluster 2
05D08
05N02
05M13
unrelated mAb
D
Cluster 1
Cluster 2
03F18 08O09 08D18 08K19 10H18
05D08 05N02 05M13 unrelated

Figure 4

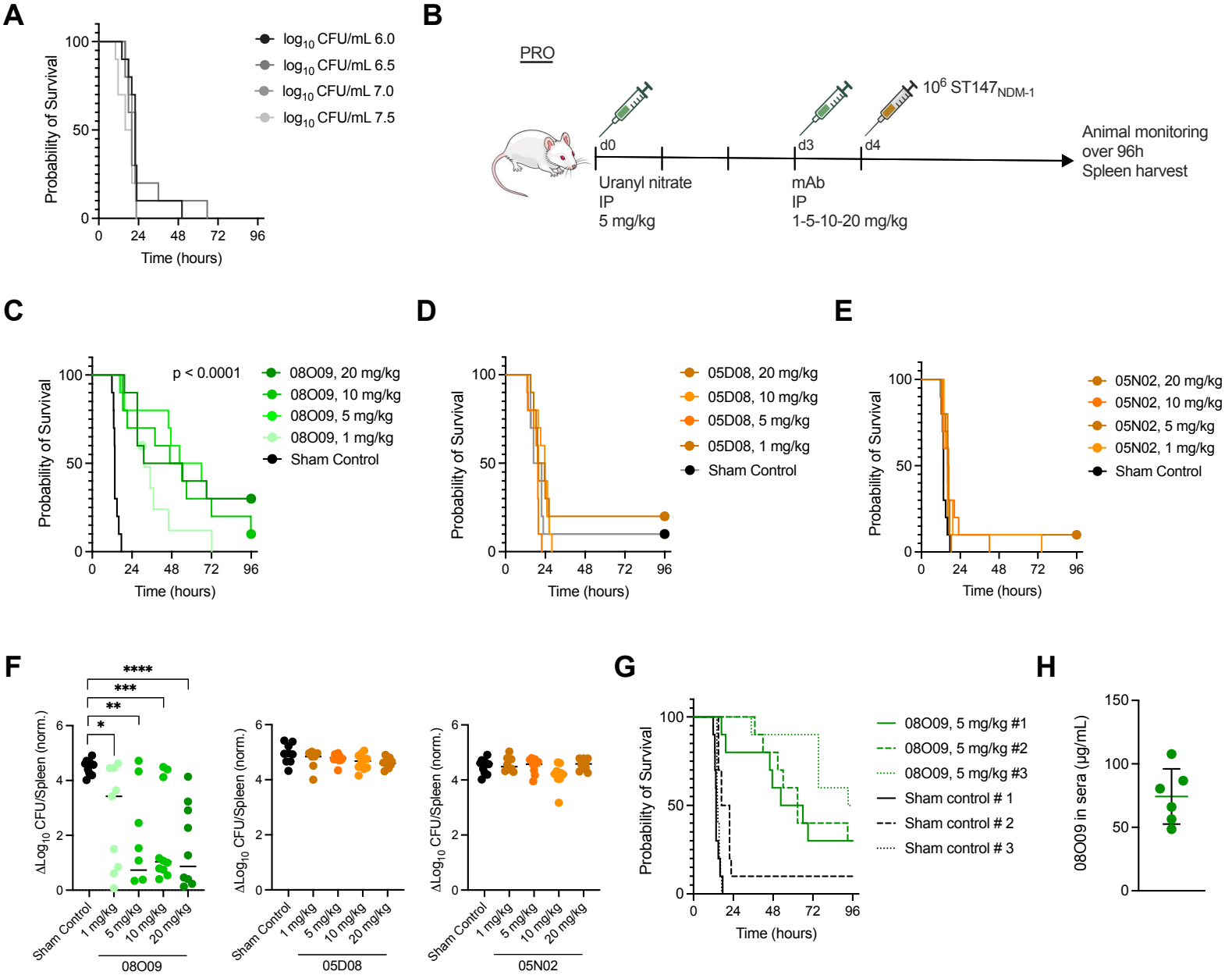
A
Probability of Survival
Time (hours)
log10 CFU/mL 6.0
log10 CFU/mL 6.5
log10 CFU/mL 7.0
log10 CFU/mL 7.5
B
PRO
d0
d3
d4
10^6 ST147NDM-1
Uranyl nitrate
IP
5 mg/kg
mAb
IP
1-5-10-20 mg/kg
Animal monitoring
over 96h
Spleen harvest
C
p < 0.0001
08O09, 20 mg/kg
08O09, 10 mg/kg
08O09, 5 mg/kg
08O09, 1 mg/kg
Sham Control
D
05D08, 20 mg/kg
05D08, 10 mg/kg
05D08, 5 mg/kg
05D08, 1 mg/kg
Sham Control
E
05N02, 20 mg/kg
05N02, 10 mg/kg
05N02, 5 mg/kg
05N02, 1 mg/kg
Sham Control
F
ΔLog10 CFU/Spleen (norm.)
Sham Control
1 mg/kg
5 mg/kg
10 mg/kg
20 mg/kg
08O09
05D08
05N02
G
08O09, 5 mg/kg #1
08O09, 5 mg/kg #2
08O09, 5 mg/kg #3
Sham control # 1
Sham control # 2
Sham control # 3
H
08O09 in sera (µg/mL)

Figure 5

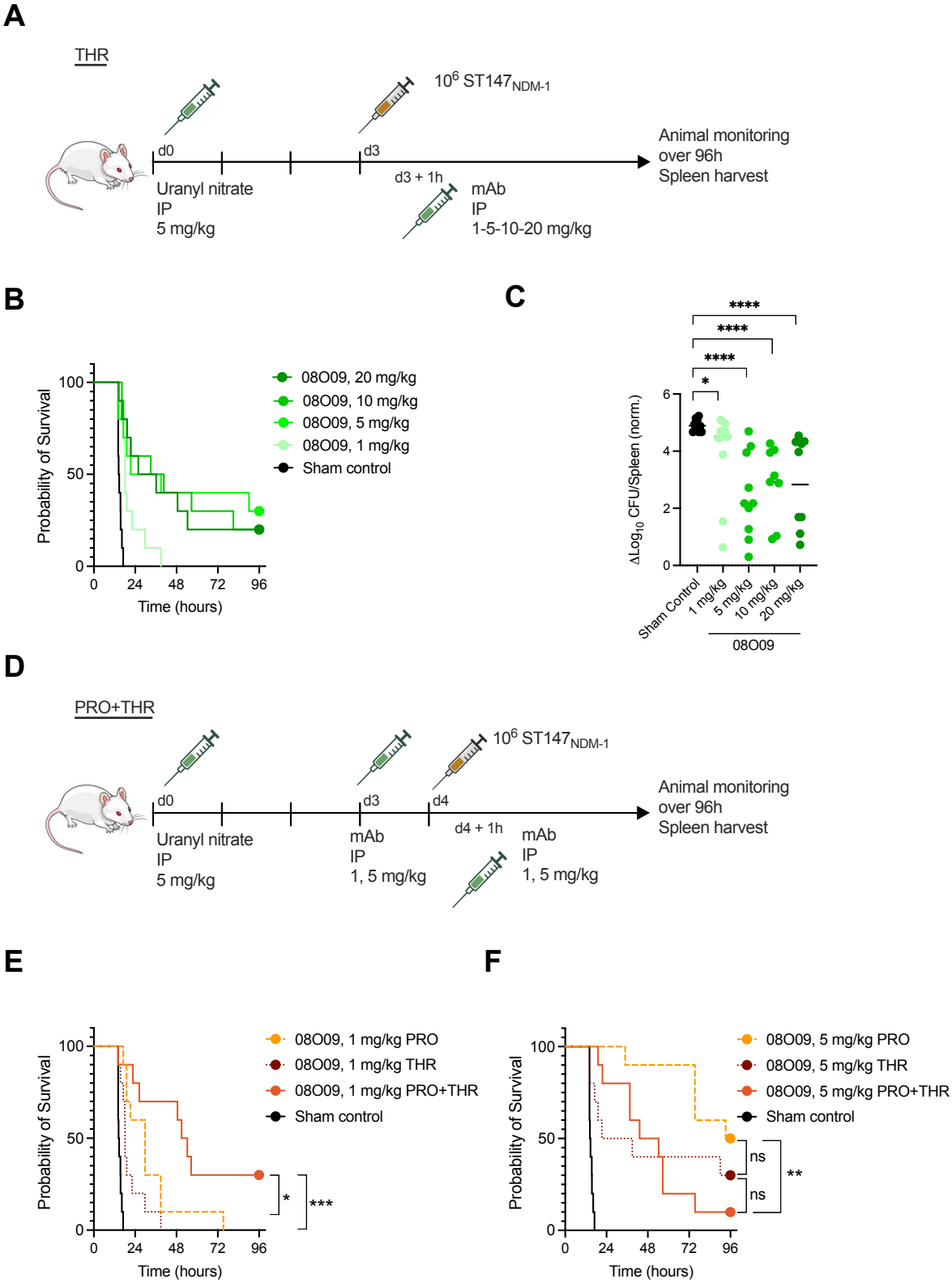
A
THR
10^6 ST147$_{NDM-1}$
d0
d3
d3 + 1h
Uranyl nitrate
IP
5 mg/kg
mAb
IP
1-5-10-20 mg/kg
Animal monitoring
over 96h
Spleen harvest
B
Probability of Survival
Time (hours)
08O09, 20 mg/kg
08O09, 10 mg/kg
08O09, 5 mg/kg
08O09, 1 mg/kg
Sham control
C
ΔLog_{10} CFU/Spleen (norm.)
Sham Control
1 mg/kg
5 mg/kg
10 mg/kg
20 mg/kg
08O09
D
PRO+THR
10^6 ST147$_{NDM-1}$
d0
d3
d4
d4 + 1h
Uranyl nitrate
IP
5 mg/kg
mAb
IP
1, 5 mg/kg
mAb
IP
1, 5 mg/kg
Animal monitoring
over 96h
Spleen harvest
E
Probability of Survival
Time (hours)
08O09, 1 mg/kg PRO
08O09, 1 mg/kg THR
08O09, 1 mg/kg PRO+THR
Sham control
F
Probability of Survival
Time (hours)
08O09, 5 mg/kg PRO
08O09, 5 mg/kg THR
08O09, 5 mg/kg PRO+THR
Sham control
ns
ns

Figure 6